Study of the Effect of Air-diffusion-channel on Separation Force in Constrained Surface Stereolithography

BY

Can Gao

M.S, Beijing Information Science and Technology University, Beijing, China, 2015

THESIS

Submitted as partial fulfillment of the requirements
for the degree of Master of Science in Industrial Engineering
in the Graduate College of the
University of Illinois at Chicago, 2018

Chicago, Illinois

Defense Committee:

Dr. Jie Xu, Chair and Advisor

Dr. Yayue Pan

Dr. Jeremiah Abiade

ACKNOWLEDGEMENTS

First, I would like to thank my advisor Dr. Jie Xu from the Department of Mechanical and Industrial Engineering at University of Illinois at Chicago. Whenever I had problems or questions with respect to my thesis project, the door to Dr. Xu's office was always open. He gave me tremendous help and steered me into the right direction over the past year.

I would also like to thank Dr. Yayue Pan who was involved in the results validation part of this project. Without her valuable guidance, it was impossible to complete this project. I would also like to acknowledge her students Haiyang He and Ketki Lichade for their contribution to the experiments.

Finally, I must express my gratitude profoundly to my spouse and parents as they provided me with firm support and encouragement during my study and research time. This thesis and research would not have been accomplished without them. Thank you.

CONTRIBUTION OF AUTHORS

Chapter 1 and 2 provide the introduction to 3D printing technology, photopolymerization, the main research question of this dissertation and the significance of this research question. Chapter 3 and 4 represent a series of unpublished simulations and experiments. Ketki Lichade assisted me in the experiments shown in Figures 20 to 23 of Chapter 4. I anticipate that this research will be continued after I graduate and that the work will be published as part of a co-authored paper. Chapter 5 presents my overarching conclusions and the future work and future directions of this project.

TABLE OF CONTENTS

TABLE OF CONTENTS (Continued)

TABLE OF CONTENTS (Continued)

LIST OF TABLES

LIST OF FIGURES

LIST OF FIGURES（Continued）

LIST OF FIGURES（Continued）

LIST OF ABBREVIATION

AM	Additive manufacturing
STL	Stereolithography
PBF	Powder bed fusion
MJ	Material jetting
BJ	Binder jetting
LOM	Laminated objective manufacturing
FDM	Fused deposition modeling
DED	Directed energy deposition
VP	Vat photopolymerization
MPVP	Mask projection vat photopolymerization
DMD	Digital micromirror device
CSVP	Constrained surface vat photopolymerization
2PP	Two-photon vat photopolymerization
PDMS	Polydimethylsiloxane
PI	Photoinitiator
M	Monomer
$P^{\cdot}$	Polymer radical
DLP	Digital light projection
LPS	Liquid-phase sintering
PDE	Partial differential equation

SUMMARY

Although constrained surface vat photopolymerization possesses fast printing speed and unrestricted building height compared to free surface stereolithography, it usually suffers from large separation forces required to detach cured parts from constrained window. To reduce the separation forces, introducing oxygen inhibition layer has recently proven to be an efficient method. Apart from conventional constrained surface vat photopolymerization, a thin layer where polymerization is inhibited continuously exists during fabrication process, hence avoiding the formation of vacuum between cured parts and vat surfaces. As a result, continuous fabrication that otherwise is challenging can be achieved. However, current methods are still not favorable to maintain oxygen inhibition layer for sufficient fabrication time. Recently, air-diffusion-channel constrained surface has been proposed for improving the stability of oxygen inhibition. Specifically, a thin layer of polydimethylsiloxane is added to the porous acrylic surface, thereby continuous oxygen supply is obtained owing to high oxygen permeability through PDMS. To better understand the mechanics behind this method and further improve its capability, simulations of the separation force and oxygen inhibition are conducted using COMSOL, a finite element analysis software. Simulation results indicate that oxygen plays an important role on separation force and there is a relationship between channel area ratio and effective printing time. Specifically, oxygen inhibition mechanics, polymerization process and oxygen diffusion through the constrained surface are comprehensively considered for an optimal structure of constrained surfaces.

Chapter 1 Introduction

1.1 Introduction to additive manufacturing

Along with rapid development of the modern society, numerous manufacturing techniques have been developed hitherto. Undoubtedly, they have been widely applied for all types of purposes such as producing merchandises and scientific exploration. Although all these techniques have the capabilities to turn raw materials into final products, the mechanisms behind them are quite different, by which modern manufacturing techniques can be broadly categorized into three types: net shape process, subtractive process, and additive process. Just as their names imply, net shape process does not add nor subtract materials from raw materials but simply involves shape changes. For instance, die casting capitalizes on forcing molten metal into a mold cavity, which is composed of two tool steel dies. After the metal solidifies again, its shape is reproduced from the mold. Despite the fact that this method produces excellent fabrication quality with good dimensional accuracy and smooth surface finishing, high cost of dies and related components have hindered its applications especially for those involve prototyping designs. Subtractive process is another type of fabrication methods that has been widely used over the past centuries. In contrast to net shape process, this method removes partial materials from original workpieces, and further obtains final shapes. To name a few, milling and drilling are two commonly used machining methods in industrial manufacturing. During the process, feeding rotary cutters are adopted to remove materials via removing undemanding materials. Similar to net shape manufacturing, subtractive manufacturing brings in good resolution and smooth surfaces. However, it usually requires more materials than what is needed, hence huge amounts of waste are indispensable [1]. Recently, the third type of manufacturing process, namely, additive manufacturing (AM) has attracted ever-increasing attention. Compared to the other two

processes, AM adds material together to create three-dimensional (3D) objects with the aid of computer control. In other words, AM allows creation of final objects from a digital model directly, thereby rapid prototyping can be easily achieved [2]. Moreover, as this method does not need to remove internal materials via cutting tools or casting via specific molds, 3D objects with complex shapes that otherwise are difficult or even impossible to create now become possible to fabricate. In addition, this process is normally done by layer by layer or points by points, thus avoiding the hindrances from spatial limitations.

Owing to the ease of creating 3D objects via AM, the term 3D printing nowadays is also widely used to refer to AM especially when low-cost personal machines have become popular after 2010 [3]. Moreover, various types of raw materials have been adopted in 3D printing, including plastics [4], metals [5], ceramics [6], biomaterials [7], composite materials [8], etc. As an example shown in Figure 1, a 3D structure with complicated geometry is printed by a commercial 3D printer (CoLiDo DIY Printer) with Polylactic acid (PLA) filaments.

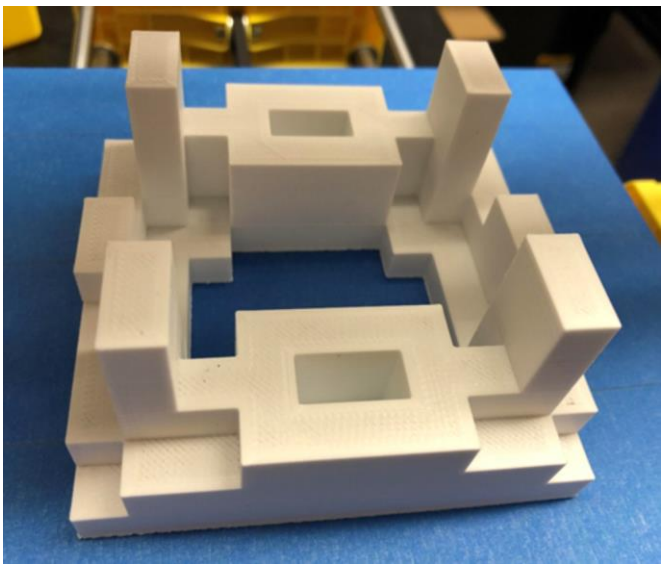

Figure 1. An example of 3D printed product

1.1.1 Generic process of additive manufacturing

As a special manufacturing technique, AM does not require either molds or cutting tools, it creates physical parts according to digital designs, namely, computer-aided design (CAD), via several steps as described below (Figure 2).

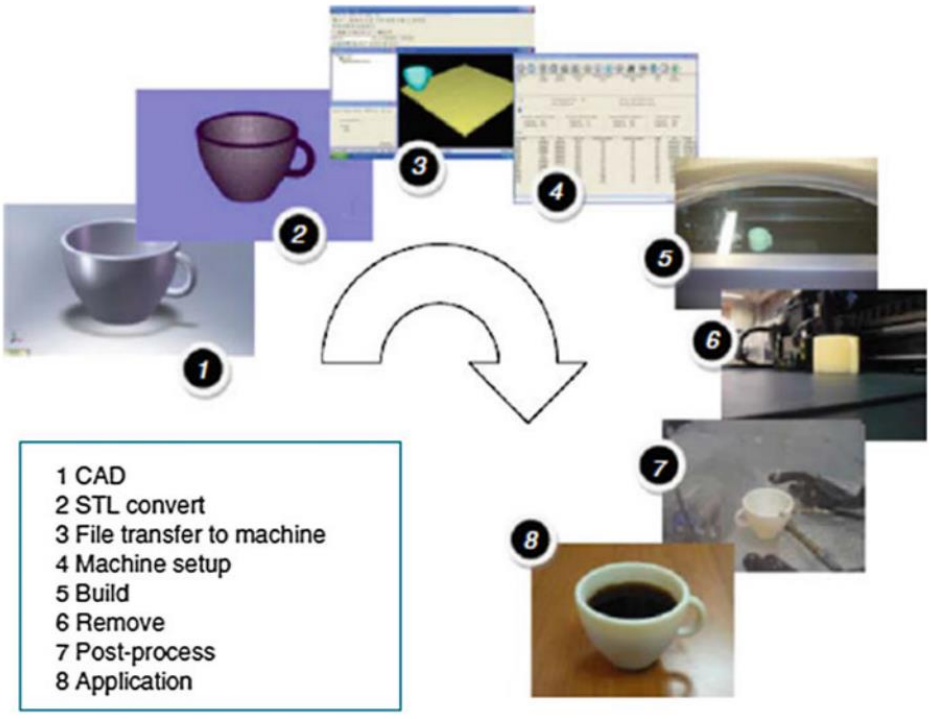

Figure 2. A schematic illustration of generic process of additive manufacturing. Adapted from [9].

1) CAD model that describe the exact external shape of the final structures is created via solid modeling software. Besides, scanning techniques such as laser scanning are other methods to generate digital models.

2) The created CAD model is then converted into a file with stereolithography (STL) format, which is widely accepted in most modern AM machines. Conventionally, STL uses many polygonal facets (mostly triangles) to represent 3D objects with any shapes. It is worth noting that the

surfaces represented by STL file should be closed and connected completely. Moreover, errors may exist when using triangular facets to create approximate models.

3) After generating the STL file, it should be transferred to AM machines. Although this step is extremely simple, it may affect the final results. For instance, one should firstly determine the build-up direction for the parts and set up the correct size scaling and position on the platform. A wise decision for the build-up direction could result in a better resolution, faster building rate, and small trapped volume. Moreover, in order to avoid rupture of final parts due to heavy and inclined parts or reduce the adhesiveness between parts and platforms, supporting structures should be added under certain circumstances. Furthermore, other parameters such as slicing distance, tool path that affect the quality and resolution of the parts should be considered and optimized as well.

4) The AM machine used should be set up properly before the real fabrication process takes place. For instance, printing parameters such as energy intensity and writing speed should be carefully adjusted in advance. Other physical requirements such as the amount of photosensitive materials, expiration date of the materials, and position of the printing platforms should also be inspected prior to the fabrication process.

5) After all the configurations for a printing process are successfully set up, one is able to start the main step in a typical 3D printing process, namely, the fabrication (printing) process. Compared with traditional manufacturing methods, building process in 3D printing is almost automated. That is, only simple operations such as replenishment of photosensitive materials, or solving power outage are required during building process.

6) The printed parts should either be removed from the platform or cleaned from excessive materials surrounded after the machine completes the building process. Herein, one

should always inspect the conditions before taking the parts off. For example, the operating temperatures should reach a sufficient low value.

7) Another key step in 3D printing is the post-processing step. Through this step, the printed parts can be cleaned up and the supporting scaffolds are removed. It is worth mentioning that as some printed parts are quite brittle and fragile, thus post-processing often involves experienced and cautious manual operations that are quite time-consuming.

8) Last but not the least, a great number of printed parts cannot be used directly after post-treatments. For instance, certain pristine parts possess weak mechanical properties that are not preferable for real applications. Thereby, other treatments such as baking or UV exposure are recommended for improving their performance. In addition, priming and painting also bring a better surface texture and an esthetic appearance to the final objects.

1.1.2 Advantages and disadvantages of additive manufacturing

As described above, AM is a completely different technique in manufacturing compared with other counterparts (i.e., net shape and subtractive manufacturing), and it has been widely considered as a revolutionary technology that may change the way how we think about manufacturing [10]. Besides, AM has already strikingly changed our life especially after personal 3D printers became easily accessible recently. All these positive statements for AM are attributed to its advantages as follows.

1) Complexity is free. Conventional 3D printing process relies on either layer by layer or point by point, thus complexity is no longer a problem for manufacturing. 3D objects with any complex shape can be sliced into multi layers and then created individually with connection. Therefore, it would be cheaper and faster to print a hollow object with complex design than a simple cube with same size.

2) Variety is free. As aforementioned, 3D printing creates any objects directly according to digital model, and the building process is almost automated. Therefore, any change for the final products could be made on original CAD designs.

3) Lead time is short. Compared with other manufacturing methods, any prototyping designs can be transferred into physical parts right away after 3D printing. Additionally, one can directly use and test the fabricated parts after simple post-processing.

4) Assembly is free. In contrast with other methods, parts created via 3D printing methods are automatically connected, thus assembly is usually not required.

5) Professional skills are not indispensable. As the building process in 3D printing is almost automated, only few interactions are required. Even an elementary child could easily learn and use a 3D printer.

6) Less waste. Typically, in a traditional subtractive manufacturing process such as milling and drilling, removed parts from original workpieces become wastes after the fabrication, giving rise to a big problem in the cost of products. On the contrary, most of the materials consumed during AM fabrication process are used for the final products, and only a small fraction of the material is wasted due to the introduction of supporting or sacrificial parts.

7) Infinite shades of materials. As various colors can be incorporated into CAD files, the final parts can be created with multi colors via typical 3D printers. It greatly saves the time for post-processing.

8) Replication is simple. With the aid of a scanning tool such as laser scanning, one can easily replicate objects with a 3D printer.

Despite many advantages elucidated above, disadvantages of AM still exist. First, building rate is still one of the major downsides exist nowadays. For example, a typical commercial 3D printer may spend several hours to print a small cube with length of 10 mm. In addition, the resolution is still not competitive compared with other methods. Although some techniques such as two-photon polymerization could result in a resolution of nanometer scale, their high cost and consumption of time hinder their broad applications. Moreover, the size that can be created via 3D printing is still very small in most cases. While bigger parts can be fabricated using a larger machine, the cost is also not preferable. Finally, mechanical properties of the parts created are also big issues when it comes to actual applications, defects and fractures of the final products are inevitable due to fragile and brittle nature of the materials.

1.1.3 Classification of additive manufacturing

Ever since the early AM machines and associated materials invented in 1980s [11], various types of principles towards different applications have been developed, including photopolymerization, electronic beam melting and so forth. In this section, main types of AM are described and discussed as follows.

1) Stereolithography (STL): STL is one of the oldest techniques for AM, and the first equipment was invented by Charles Hull in 1986 [12]. The process of STL capitalizes on the light to convert liquid photosensitive materials into solid parts. Specifically, the manufacturing process of a typical STL is based on photopolymerization on photosensitive resins.

2) Powder Bed Fusion (PBF): The first commercialized PBF process is Selective laser sintering (SLS). Four fusion mechanisms have been developed nowadays for PBF processes, including solid-state sintering, liquid-phase sintering (LPS), chemically induced sintering, and full melting. All these PBF processes involve a basic mechanism. That is, there should be at least one

thermal source to induce fusion between particles, a controlling method for powder fusion in a prescribed region of every layer and different approaches to add and smoothen powders for each layer[9].

3) Material Jetting (MJ): MJ is a process in which all the materials in droplet format is jetted from printing head or multi jetting heads to fabricate parts layer by layer. Only a limited list of materials could be used in MJ, such as waxy polymers, acrylic polymers, ceramic and metals. Moreover, to facilitate the droplet formation, solid materials should be liquefied upon heating; besides, the viscosity must be adjusted to an acceptable low value for jetting when it comes to fluids with high viscosity. It is worth mentioning that the viscosity is the most problematic aspect for MJ.

4) Binder Jetting (BJ): BJ is developed by MIT in the early 1990s, in which binders are added onto powder bed after one layer of the final part forms. In the meanwhile, the powder bed gradually moves down, followed by spreading a new layer of powders on the top using a counter-rotating roller mechanism, which is similar to the mechanism used in PBF. In general, the parts fabricated using BJ possess a lower accuracy than those created using MJ. However, BJ owns its own advantages. To name a few, BJ enables the creation of colorful parts and favorable material combination, which is difficult to achieve using other methods. Additionally, BJ process is much faster than MJ as less materials is jetted during the fabrication. Lastly, BJ has the capability to create ceramic and metal parts with good quality.

5) Laminated objective manufacturing (LOM): A variety of materials have been developed for LOM, including papers, plastics, ceramics, and metals. Based on different bonding methods, LOM technique can be divided into four categories: gluing or adhesive; clamping; thermal bonding; and ultrasonic method.

6) Material extrusion: This method capitalizes on the materials that can be molten and liquefied. Generally speaking, a reservoir is used to store solid materials and the molten materials in the form of wire can be forced out when applying the pressure. In order to build a 3D parts, sophisticated plotting of the wires under a predefined path is achieved using numerical control. In addition, when the geometry of parts is complex or difficult to achieve directly, support materials are usually added. During the fabrication process, wires are bonded together after extruding out and become solid by means of automatic cooling or chemical reactions. As a simple material extrusion method, fused deposition modeling (FDM) has become very popular all over the world due to the fact that it can be realized using rapid setup and cheap raw materials. However, the accuracy and quality of final products are relatively poor compared to other advanced techniques.

7) Directed Energy Deposition (DED): The mechanism of DED is similar to that of the SLS process, yet it does not involve a powder bed. DED is a process that uses laser or electron beam based heat sources to melt material powders or wires that are fed through nozzles. Although different materials such as polymers, ceramics and metals can be used for DED, the method is mainly adopted for metal powders. In addition, the main limitation of DED lies in the poor surface quality and resolution However, these drawbacks can be improved by means of adjusting the laser power and scan speed. Hence, an optimum configuration between build speed, accuracy and size is necessary.

1.2 Introduction of Vat Polymerization

Generally speaking, vat polymerization (VP) capitalizes on the photopolymerization, by which liquid, radiation-curable materials become solid upon the introduction of light in a vat where the process happens. At present, STL has become one of the most commonly used VP

techniques, and it usually refers to microscale laser scan vat photopolymerization. Unsurprisingly, this technology has received great attention and applied in a number of fields, such as do-it-yourself handcraft 3D printing [13], biology engineering [14-16], energy materials [17], chemistry vessels [18], molecular modeling [19, 20], and microfluidic devices [21]. Typically, three different approaches have been proposed for photopolymerization processes based on different light sources: vector scan, mask projection and two-photon (Figure 3).

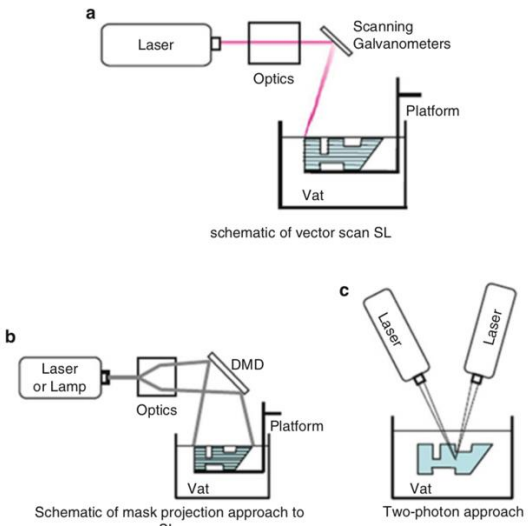

Figure 3. Three approaches to photopolymerization process.

Adapted from [9] with permission.

Vector scan micro-vat photopolymerization is a point-wise process, in which laser beam or X-ray are adopted for scanning photosensitive materials. Hereby complex shaped parts are created point by point. Conventionally, the length of final parts is smaller than 10 mm. This method was first published in 1993 by of Ikuta and Hirowatari [22]. In their work, a 5-μm diameter laser spot was used. To date, various devices have been developed using this technology, including flexible microactuators, microfluidic devices[23], manifolds, and tubes. For example, it was used to bind gears on a substrate by Takagi and Nakajima[24].

On the contrary, mask projection VP (MPVP) technology projects bitmaps of curing spots to the surface of photosensitive materials layer by layer. Hereby the curing time of mask projection VP is much faster than vector scan method since the entire cross section of the final parts can be cured simultaneously. That is, this method uses a layer-wise process instead of the point-wise one. In addition, the mask images projected by light projection devices are dynamic, and controlled by digital micromirror devices (DMD). DMD is a pivotal device that improves the speed of curing. It is composed by up to 1 million mirrors that could be turned on or off according to corresponding pixel status simultaneously [25]. At present, two types of MPVP have been developed and widely used, namely, the bottom-up and top-down MPVP (Figure 4). The bottom-up MPVP is also called constrained surface vat polymerization (CSVP) and constraint surface stereolithography.

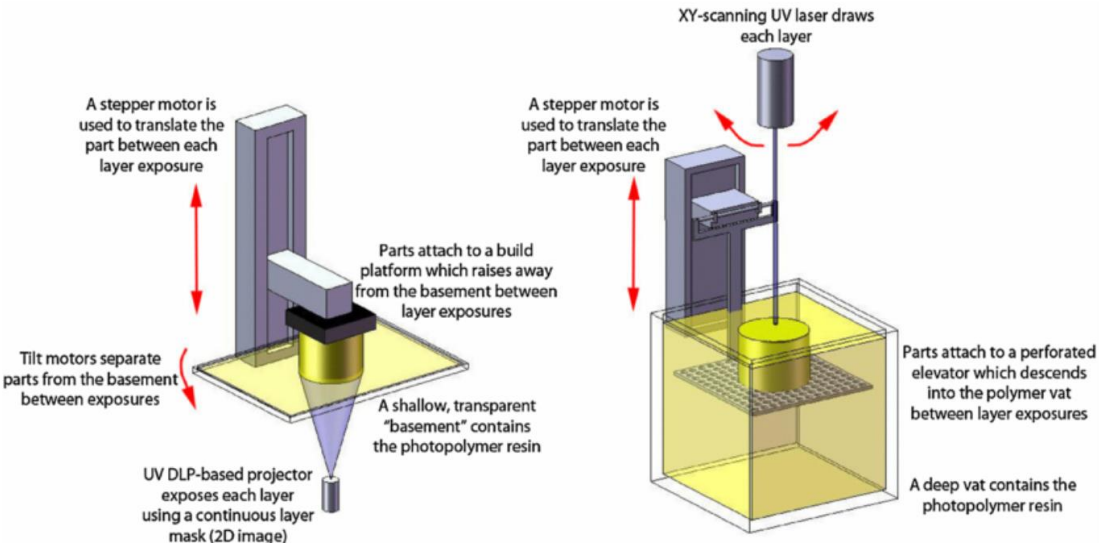

Figure 4. Two commonly used types of MPVP. a) Bottom-up MPVP; b) Top-down MPVP. Adapted from [26].

Furthermore, two-photon vat photopolymerization (2PP) capitalizes on using two photons simultaneously to strike the photoinitiator in the liquid before it decomposes, hence initiating the photopolymerization process. Owing to non-linear absorption, this method greatly improves the resolution of final part, hence it has been used for various applications [27-29]. However, it is also because of the extremely high resolution, the fabrication time can be drastically long if the final parts are too large, thus inhibiting its broad use.

1.2.1 Advantages and disadvantages of CSVP

It is worth mentioning that MPVP possesses a number of advantages and limitations. For instance, it usually gives rise to good dimensional accuracy and surface finishing. Moreover, MPVP accepts a variety of light sources including lases, lamps and LEDs with different sizes. MPVP possesses a much faster fabrication speed compared to other laser scan SLs, since it can incorporate DMD technology, by which the entire cross section of final parts can be cured. It is worth noting that there is a tradeoff between the size of cross section and final resolution, owing to the limitation of micromirrors. For example, a maximum 96 by 54 mm projection area can be achieved for a 50 μm resolution. Another limitation of MPVP is its requirement of using liquid photopolymers. Hence, the materials are limited to acrylates or epoxies. Lastly, the mechanical properties of the cured part might decay over time.

Figure 4a shows a typical CSVP, where a thin layer of liquid in the gap between the platform and vat is cured by the light projected from bottom. Afterwards, the platform and the cured part is lifted up a small distance, allowing the liquid resin fills the gap smoothly. Then they move down and keep only a thin layer liquid in the gap, in which the photopolymerization occurs. During the fabrication, this process continues until the whole part is created [30]. On the other hand, in the top-down VP, a thin layer of final part is fabricated by curing the photosensitive

materials near the top surface using a laser beam or DLP method. After that, the platform moves down a small distance, and the newly formed liquid surface is exposed to light again. The final part is fabricated by repeating this process.

As shown in Figure 4, the part height of CSVP method is not limited by the vat size. Moreover, as the photopolymerization does not take place near the resin surface, resin can be cured faster with less material waste and higher resolution compared to top-down MPVP, which arise from uncontrollable replenishment of the fresh resin on the top surface. However, CSVP is not impeccable. That is, significant pull-up forces are required to separate the cured part from vat after each layer is solidified, due to the fact that cured parts have to be separated from the vat bottom for the replenishment of fresh resin. As a result, the over-large forces would lead to the damage of printed part and the constrained surfaces shown as Figure 5.

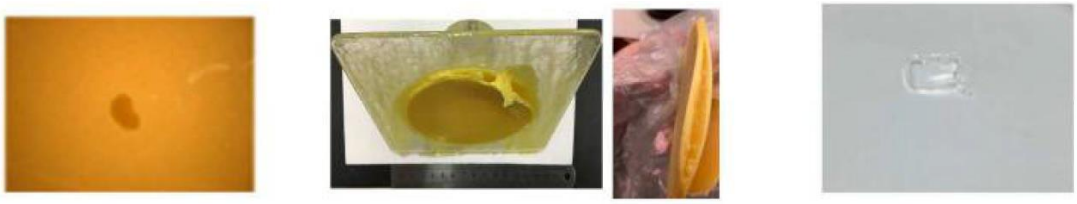

Figure 5. Damage caused by large separation force.

Adapted from [31] with permission.

1.2.2 Methods to decrease separation force

The separation process of cured part from the vat is illustrated in Figure 6, the newly cured layer is sandwiched between the early cured part and the bottom of the vat, which is covered with coating medium for reducing the separation forces. While the platform moves up, the separation process initiates at the boundary of the interface between cured parts and the coating medium (Figure 6b). In the meantime, the separation force grows up during the

movement of the platform. Finally, the force gradually reduces until the separation completes as shown in Figure 6d.

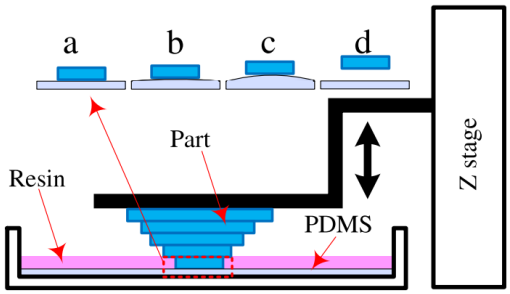

Figure 6. Separation process in CSVP.

Adapted from [30] with permission.

During the lifting-up process, the newly cured layer may not be bonded with the cured part but attached to the bottom of the vat because of the large adhesion forces between the coating medium (e.g., PDMS in Figure 6) and cured layer. As a result, it compromises the coating medium and the cured parts. Given this concern, several approaches have been proposed to resolve this issue.

One of the most common approaches to tackle this problem is coating a suitable medium on the bottom surface of the vat such as PDMS film, Teflon film[32, 33]. This can be attributed to smaller bonding strength between the cured parts and coating medium, hence moderating the separation process. This advantage comes from the high oxygen permeability of PDMS, which results in an oxygen inhibition layer formed above the PDMS, hereby preventing the cured layer from being attached on the bottom of the vat [34] as shown in Figure 7.

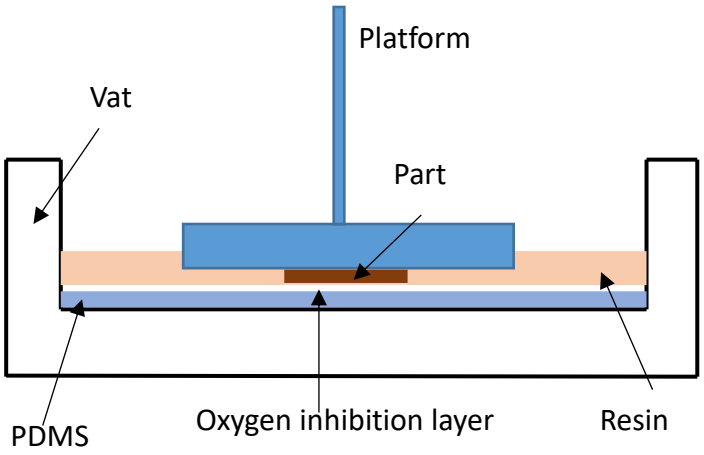

Figure 7. Scheme of oxygen inhibition layer above PDMS.

A Perfactory System was developed by EnvisionTEC company to reduce the separation force by moving up one side of the platform slowly to peel the cured part from vat than pulling that up [9]. But this method only works for the parts cured close to the tilting side of the platform. Moreover, a two-way motion system was designed based on the two approaches described above [35]. Its schematic illustration is shown in Figure 8. Specifically, after one layer is cured, the platform moves up only by a layer thickness. Since the existing of oxygen inhibition layer works as the lubricants, the tank can be easily moved along X direction, followed by a new layer being cured then. By this approach, the separation force can be reduced significantly, however, the extra motion may increase the building time and lead to the deformation of part in horizontal direction.

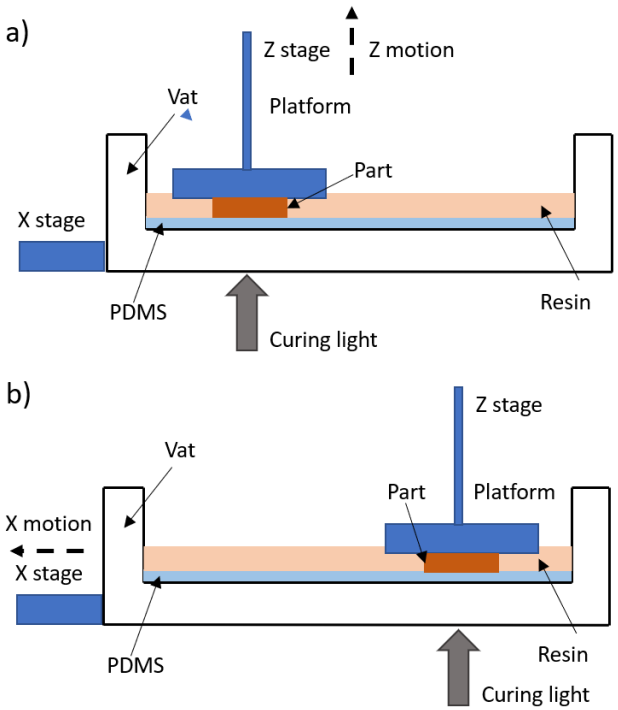

Figure 8. Scheme of two-way motion system.

Recently, Tumbleston and co-workers have successfully increased the building speed by 25-100 times compared to commercial machines by adapting an oxygen-permeable window (Teflon AF 2400 film) as the bottom of the vat as shown in Figure 9 [36]. However, this design would lead to the crease of the films because of low stiffness.

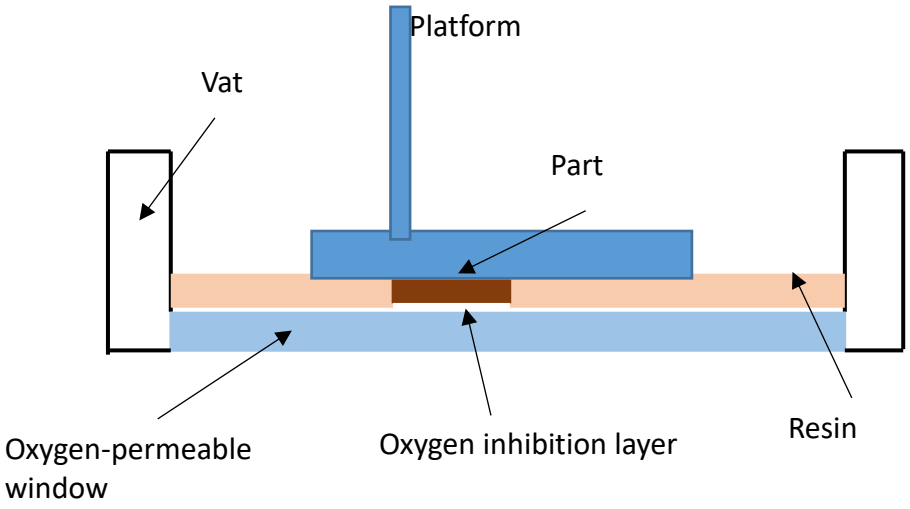

Figure 9. Scheme of configuration for CSVP with oxygen-permeable window.

1.3 Scope of this project

The separation force is known to be responsible for failures during the fabrication processes, such as creeping on the surface of the cured parts. Herein, a variety of methods have been developed to decrease the separation force and improve the fabrication quality, such as adding a sliding mechanism to separate cured parts from the bottom of vat [25, 37], and imparting oxygen inhibition layers. It has been recently found that oxygen plays an important role in decreasing separation force [31, 36], giving rise to several approaches to decrease the separation force, including coating [38, 39] vat surfaces with polydimethylsiloxane (PDMS) (Figure 7), or the use of oxygen permeable films (e.g., Teflon AF 2400) [36] as constraint surfaces. Although highly-oxygen-permeable films are the good options for creating oxygen inhibition layers, they often suffer from various challenges such as bending and creasing due to softness. Given these concerns, air-diffusion-channel substrate covered with PDMS (Figure 10b), has been proposed [40] to maintain good oxygen permeability while improving the mechanical performance of the films. It has been found that the air-diffusion-channel incorporated substrate (Figure 10b) has a higher bonding strength between PDMS and substrate and an enhanced oxygen inhibition effect

than the conventional design (Figure 10a). To further investigate and understand the fundamental principles behind this novel design, we have conducted simulations on the effect of the air-diffusion-channel structure towards decreasing the separation force for constrain surface stereolithography process.

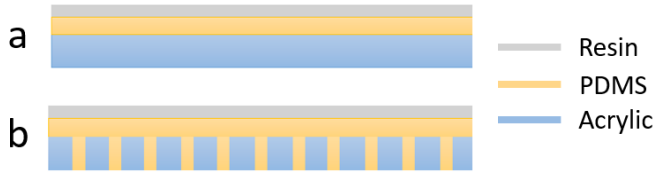

Figure 10. a) Conventional design of constraint surface. b) Air-diffusion-channel design of constraint Surface.

In the following chapters, several models that are adaptable to represent the oxygen permeable and photopolymerization occurring in constraint surface stereolithography printing process and capable to illustrate effect of oxygen on photopolymerization and separation force are presented. Chapter 1 depicts the introduction of stereolithography and the advantages of constraint surface stereolithography. Chapter 2 represents the main photopolymerization mechanisms behind the fabrication process, how oxygen inhibition works and how to simplify the photopolymerization mechanisms for simulations. Chapter 3 introduces the simulation physics, modeling process and validates the photopolymerization process. Chapter 4 studies the effect of oxygen-diffusion-channel and area ratio of holes to surface on the separation force.

Chapter 2 Basic mechanism for photopolymerization

Based on the difference of mechanisms for polymerization, this process is classified as step polymerization and chain polymerization. The largest difference of chain and step polymerization is the species that can react with each other, that is, the major monomers in chain polymerization process containing carbon-carbon bonds (also termed as vinyl monomers) [41]. The size of polymer molecules formed by step polymerization increases relatively slowly compared to that of the chain polymerization. Step polymerization proceeds by stepwise reactions between different functional groups of reactants such as monomers, dimers, trimers, tetramers, pentamers, and hexamers, until large size molecules have been formed. On the contrary, the mechanism behind the chain polymerization is quite different. Specifically, reactive species with reactive center are produced by initiators, followed by propagating the reactive center through successive reactions with large numbers of monomers in chain polymerization.

As one of the chain polymerization, photopolymerization has great advantages on rapid curing speeds at room temperature, including better energy efficiency, and lower concentration of volatile organic compounds [42]. Photopolymerization is defined as a process where the reactions of monomers produce solid polymeric structures by light irradiance and polymerization [43]. There are two main types of photopolymerization: free-radical type and cationic photoinitiation type. Free-radical polymerization usually uses acrylates with high reaction rates and accepts a lot types of monomers and initiators; On the other hand, cationic photopolymerization commonly take advantages of epoxides, which are not interfered by oxygen inhibition and possess lower toxicity and shrinkage.

2.1 Free-radical photopolymerization mechanism

Free-radical photopolymerization is a chemical chain reaction process involving three sequential steps – initiation, propagation, termination. Besides, oxygen inhibition may also occur if it is present in the system. A typical radical chain photopolymerization occurs when radicals are created upon the irradiation of visible light, laser and ultraviolet light. The reactants in the photopolymerization reaction process for a typical CSVP system are photoinitiator (PI), monomers (M), and oxygen (O_2).

The main reactions in a typical photopolymerization process are shown in Table 1:

TABLE I. PHOTOPOLYMERIZATION REACTIONS

Reaction	Scheme
Photoinitiator dissociation	$\mathrm{PI} \xrightarrow{k_d} 2R^{\cdot}$
Chain initiation	$R^{\cdot} + M \xrightarrow{k_p} P^{\cdot}$
Chain propagation	$P^{\cdot} + M \xrightarrow{k_p} P^{\cdot}$
Chain termination	$P^{\cdot} + P^{\cdot} \xrightarrow{k_t} P_d$
Inhibition	$P^{\cdot} + O_2 \xrightarrow{k_o} P_d$

First, photoinitiator molecules are decomposed and form initiator radicals when the light exists (Photoinitiator dissociation). These radicals then react with monomer molecules freely, forming polymer chains ($P^{\cdot}$) (Chain initiation). Afterwards, the polymer chains grow via reacting with monomers or other polymer chains, under a given reaction rate k_p. This process is called chain propagation. Besides, polymer chain stops propagating and terminates. Termination occurs at radical center with its annihilation by reactions between radicals. Two radicals can be terminated either by combination or disproportion at a rate of k_t. Finally, oxygen may also react with polymer chains, hence inhibiting the propagation and terminating the processes at a rate of k_o.

It is found that the initiation rate of photopolymerization can be very fast and controlled by a combination of the radicals, light intensity and so force. The reaction rate according to Beer Lambert Law is as follows [44],

$$k_d = \beta I_o e^{-(\varepsilon[PI]z)} \tag{2.1}$$

where $[PI]$ is the concentration of initiator; I_o represents the light intensity; β is photoinitiation coefficient [45, 46]; ε is determined experimentally, represents the molar absorption of photons [47]. Additionally, the initiation includes two steps, catalyst dissociation and chain initiation. The latter part is the beginning of propagation, in which the radicals react with the monomers to produce the chain-initiating polymers.

Moreover, k_p is the rate constant of propagation, and its value is usually very large, which is in the range of 10^2 to 10^4 $L \cdot mol^{-1} \cdot s^{-1}$[41]. Propagation of chain polymers stop at some point and terminate. Termination occurs if two polymer radicals combine with each other. Typical termination constant is in the range of 10^6 to 10^8 $L \cdot mol^{-1} \cdot s^{-1}$ [41] or greater than the propagation rate k_p. Nevertheless, the rate constant of termination is greater than the propagation rate, but the termination cannot prevent propagation since the polymer radicals for that are in a very low concentration.

2.2 Oxygen inhibition effect upon free-radical photopolymerization

As aforementioned, free-radical photopolymerization can be inhibited by oxygen molecular as shown in Figure 11. The oxygens have the capability to quench the active triplet photoinitiator and scavenge initiators and polymer radicals via the reactions with them [41, 48-50]. This problem has affected the application of free-radical photopolymerization on thin films coating and inhibited the photopolymerization of UV-curable resin in air. Thus, efforts have been focused on addressing this problem by understanding the oxygen inhibition mechanism towards

free-radical polymerization to enable its application and improve the quality of final products. At present, different methods have been developed to solve the oxygen inhibition problem by preventing oxygen from entering the system such as using waxes or inerting equipment, thus offering a higher concentration of initiator to increase the oxygen consuming speed, or adding other chemical additives like amines to capture oxygen molecules [51]. However, the above methods have strong drawbacks such as increasing the manufacturing cost or leading to product quality problems. For example, high concentration of initiator usually results in the decrease of light penetration depth and low conversion, which further affect the quality of cured parts.

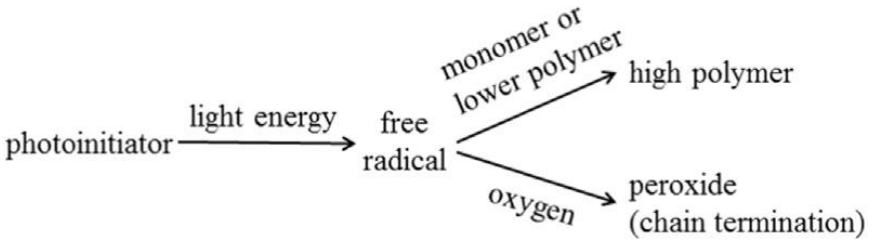

Figure 11. Oxygen inhibition in photopolymerization.

Adapted from [52]

However, if we think this problem in another way, oxygen inhibition can be used to promote the CSVP print process. Specifically, when the stereolithography is built on an oxygen-permeable tank (vat) window, or the tank is coated with a layer of high oxygen concentration PDMS, a thin layer of uncured polymer liquid between the window and the cured part would work as a thin layer of lubricant to lower the separation force as shown in Figure 12, an oxygen-permeable window is used in ceramic 3D printing.

There are certain substances can suppress the polymerization process by reacting with the initiators and propagating radicals, and further convert them into dead polymers. Among them, oxygen is known as a convenient and strong inhibitor that has been greatly adopted in CSVP

for realizing continuous printing ability, and its mechanism of inhibition is expressed as the inhibition step in TABLE I. Generally, oxygen molecules diffuse into the vat freely from surrounding air through the constrained window, and then they can react with radicals thus inhibiting the polymerization process. This reaction-diffuse process maintains an un-cross-linked layer called "dead zone" or "lubrication layer".

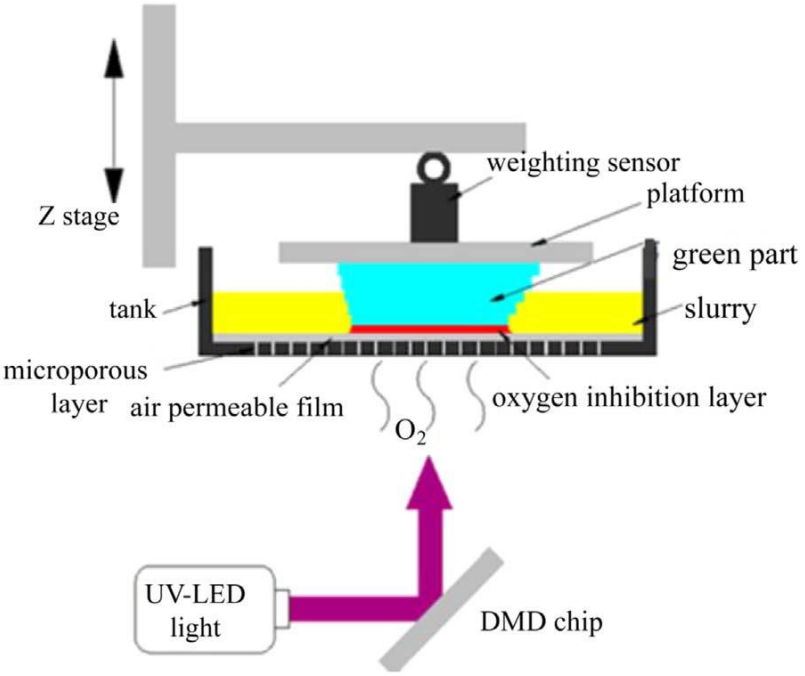

Figure 12. CSVP with oxygen-permeable window.

Adapted from [52]

2.3 Rate of polymerization and conversion limit

A large number of monomer molecules are converted to polymers during the propagation step by reacting with the initiating radicals produced in initiation step. To obtain an expression of the rate of polymerization, an assumption that k_p and k_t are independent is made. The process for the consumption of monomers in chain initiation and propagation steps is showed in TABLE I. The rate of monomer consumption is illustrated as,

$$\frac{-d[M]}{dt} = R_i + R_p \quad (2.2)$$

where R_i denotes the initiation rate and R_p represents propagation rate. Considering that the number of monomer consumed in initiation step is lower enough to be neglected, the first tern then is neglected. Thereby the polymerization rate can be expressed as equation 2.3:

$$R_p = k_p[M][P^{\cdot}] \quad (2.3)$$

In the above equation,$[M]$ represents monomer concentration, $[P^{\cdot}]$ means the overall concentration of the polymer radicals produced in propagation step.

The degree of cure in photopolymerization process is estimated based on that the assumption that gel is considered as an infinitely insoluble large molecule [53], which is represented by monomer conversion (equation 2.4). Initial concentration and the concentration of monomer after photopolymerization are represented as $[M_0]$ and $[M]$, respectively.

$$\text{Conversion} = \frac{[M_0]-[M]}{M_0} \quad (2.4)$$

Therefore, the cured parts are determined by comparing the local conversion value and the critical conversion limit. According to reference [44], the critical conversion limit is defined as 12%.

Chapter 3 Study of resin curing process

In this section, a two-dimensional (2D) model is created to simulate resin curing process and how the oxygen inhibition works during this process. The model is composed of three domains: the acrylic substrate, PDMS (oxygen feed side) and resin (polymerization reaction zone) domains (Figure 12).

Since the oxygen permeability of the acrylic substrate is relatively low, the oxygen transportation in acrylic is neglected in this model. Oxygen transportation process (Figure 13) and photopolymerization are coupled in this simulation.

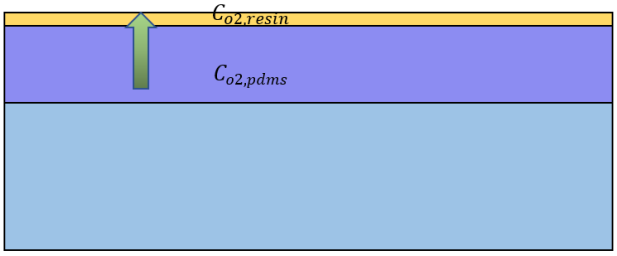

Figure 13. Domains and boundaries used in the model and oxygen transport.

3.1 Introduction of COMSOL

COMSOL Multiphysics is a simulation software that offers a cross-platform, multiphysics environment and solvers for finite element analysis. It is adaptable for conventional physics-based user interfaces and versatile for coupled systems, and provides an integrated development environment and unified work procedure for mechanical, fluid, chemical engineers and electrical, etc.

Generally, model building for the simulation of oxygen inhibition in COMSOL can be divided into three steps: firstly, space dimension (2D) is set for the model space (Figure 14).

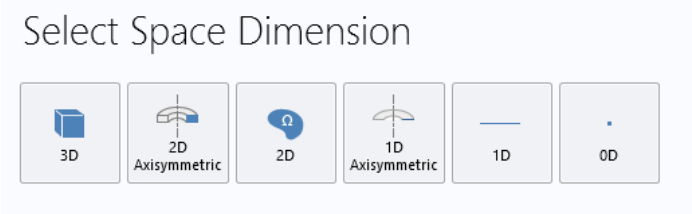

Figure 14. Model space dimension definition.

The second step is the most critical one — choosing an appropriate physics environment for the mechanism with respect to oxygen permeation and photopolymerization. Here, "Transport of Diluted Species" under the "Chemical Species Transport" (Figure 15a) was chosen as the physics environment. The last step is the configuration of preset studies. Because of the dynamic oxygen transportation and photopolymerization reaction process, time dependent study was selected as shown in Figure 15b.

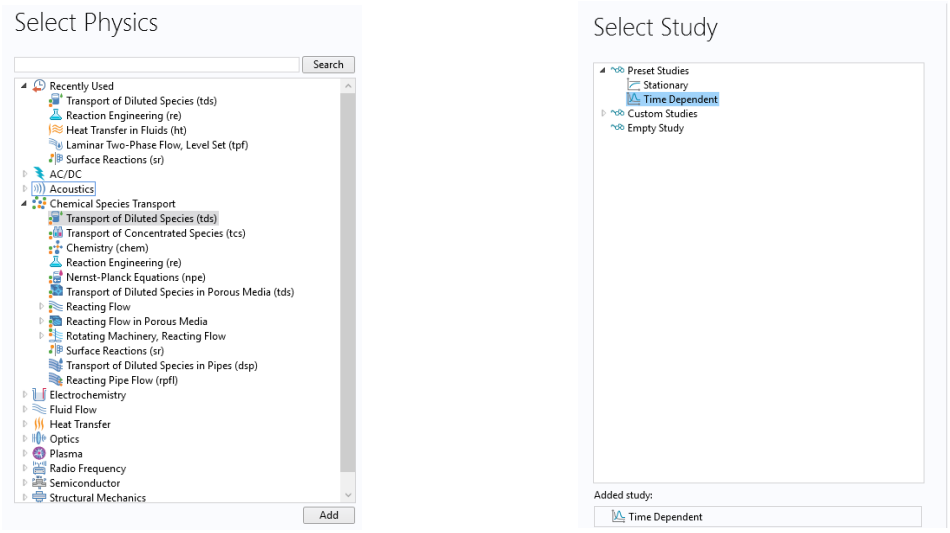

Figure 15. a) Physics Selection. b). Study Selection.

After all the three steps were set, COMSOL was ready for creating the model. A complete COMSOL model is composed by 7 parts: definition, geometry, physics, mesh, study and result.

Definition step describes global and local definitions features, such as geometric features for model. Depending on geometric scope, features are added in this section under either Global Definitions node or local Definitions node. Geometry modeling provides many ways such as solid modeling, boundary modeling, importing external CAD data etc. to create geometries in 1D, 2D or 3D. Physics consist of predefined user interface with set up equations and variables for physics in domains, boundaries, points, etc. of models, for the predefined PDEs. PDEs are equations set up for specific physics following material properties, boundary conditions of a given problem. Mesh part is where you create and control the mesh of model. Study consists of study steps which are used to control which physics interface and meshes are used for which result. Result means result evaluation and visualization, which offers numerous data analyzing tools to produce graphics and export etc.

3.2 Oxygen transport module

The interface of Transport of Diluted Species module was mainly used to help us model and simulate mass transfer in flux vector via diffusion according to the Fick's law. In this interface, mass balance equation (3.1) was applied for the study of the transportation of chemical species through diffusion.

$$\frac{\partial c}{\partial t} = \nabla \cdot (\mathrm{D}\nabla \mathrm{c}) + \mathrm{R} \tag{3.1}$$

The notations involved in equation 3.1 are explained as follows:

- c means the species concentration (mol/m^3)
- D is the diffusion coefficient of species (m^2/s)
- R is a reaction rate expression for the species (mol/(m^3·s))

In equation (3.1), the term on the left-hand side represents the accumulation of species, and the first term on the right-hand side denotes the diffusion transportation from the interaction

between the diluted species and solvent. The final term represents a source accounting for chemical reaction.

Herein, we applied Transport of Diluted Species module as the physics interface for oxygen transportation from air to PDMS (transport of diluted species1), and the transportation from PDMS to the resin (transport of diluted species2) (Figure 11).

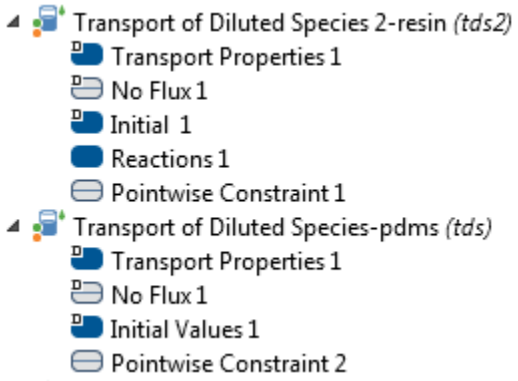

Figure 16. Physics module.

3.3 Modeling process

The modeling processes of this resin curing simulation includes geometry modeling, physics interface setting up and meshing, the details are presented in the below sections.

3.3.1 Geometry modeling

The geometry model built in COMSOL is shown in Figure 17, it consists of resin, PDMS and acrylic substrate.

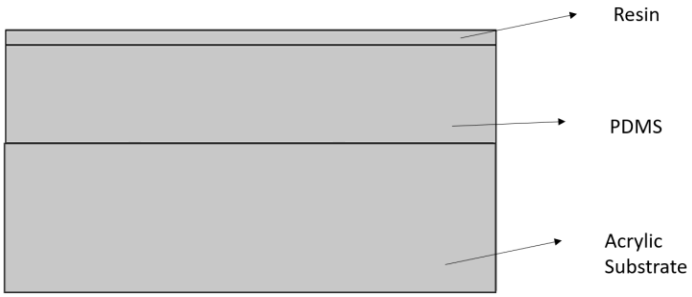

Figure 17. Conventional Geometry model

Geometric features of this model set up in global definition section as shown in TABLE IV, which are coming from tanks used in experiments. The size of tank used in experiments is 120mm X 120mm, thickness of acrylic substrate is 3mm, PDMS is 2mm. To simplify the simulation process and save the calculation time, part of the cross-section of real tanks are converted into 2D models in COMSOL.

TABLE II. PARAMETERS PRESET IN GLOBLE DEFINITION

Parameter	Value	Description
th_pdms	2[mm]	Thickness of PDMS
wid_pdms	12[mm]	Width of PDMS
th_resin	0.3[mm]	Thickness of resin
th_acrylic	3[mm]	Thickness of acrylic substrate

3.3.2 Physics module

Physics consist of predefined user interface with set up equations and variables for physics in domains, boundaries, points, etc. of models. As shown in Figure 16, the Transport of Diluted Species are used in the PDMS domain and resin domain. Material properties, boundary conditions, domain physics are set up for each domain separately.

For PDMS domain, there is only variable of oxygen concentration is considered in domain and boundary physics, which is named as c_pdms as shown in Figure 18. The initial concentration

and diffusivity of oxygen in PDMS are shown in TABLE III. The boundary conditions for the Transport of Diluted Species in PDMS are shown in TABLE IV. The boundary notations of the model are marked in Figure 19. The PDMS is insulated at bottom, but it is periodic at side walls.

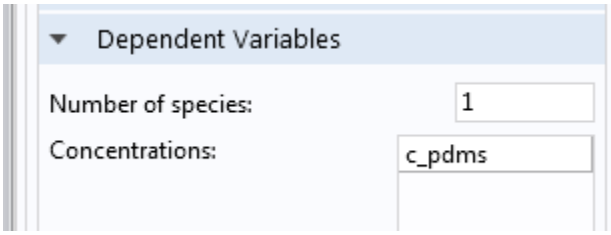

Figure 18. Variables in PDMS domain

TABLE III. PDMS PARAMETERS

Parameters	**Value**	**Description**
$C_{o2,pdms}$	4 mol/m^3	Equilibrium oxygen concentration in PDMS[54]
$D_{o2,pdms}$	3.5e-9 m^2/s	Oxygen diffusivity in PDMS[54]

TABLE IV. BOUNDARY CONDITIONS OF PDMS DOMAIN

Boundary Conditions	**Description**
n·N=0	@Y=y1, Insulation
-n·$N_{src} = n{\cdot}N_{dst}$	@X=0, X = x1, Periodic Condition

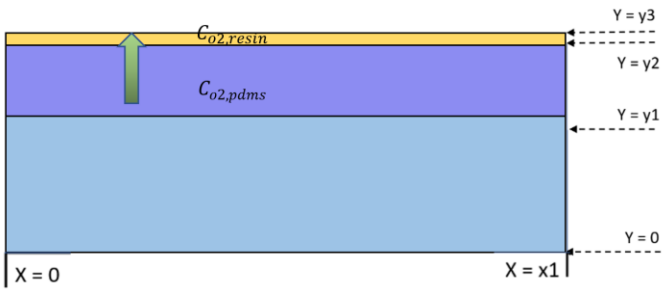

Figure 19. Boundary definition and oxygen transportation route

In resin domain, oxygen transportation and photopolymerization are coupled inside. The initial concentration of oxygen, initiator, monomer and the boundary conditions of resin domain are shown in TABLE V.

TABLE V. a) RESIN PARAMETERS b) BOUNDARY CONDITIONS

a)

Parameters	**Value**	**Description**
$C_{o2,resin}$	1 mol/m^3	Equilibrium oxygen concentration in PDMS[54]
$D_{o2,resin}$	1e-10 m^2/s	Oxygen diffusivity in Resin[55]
C_I	200 mol/m^3	Initial concentration of photoinitiator[54]
C_M	3200 mol/m^3	Initial concentration of monomer [54]

b)

Boundary Conditions	**Description**
-n·N=M$\lvert C_{o2,resin} - K_2 C_{o2,pdms} \rvert$	@Y=y2, Stiff-spring Continuous Flux
n·N=0	@Y= y3, Insulation
-n·$N_{src} = n \cdot N_{dst}$	@X=0, X= x1, Periodic Condition

In resin domain, oxygen transportation is governed by stiff-spring boundary condition (TABLE V b) and Fick's law together (equation 3.1). The photopolymerization reactions are defined in domain physics, they are illustrated as the species accumulation in TABLE VI and Figure 20, the reaction constants are show in TABLE VII.

TABLE VI. REACTIONS IN RESIN DOMAIN

Reactions	**Description**
$\frac{d[PI]}{dt} = -k_d[PI]$ $\frac{d[R^{\cdot}]}{dt} = 2k_d[PI] - kp[M][R^{\cdot}]$ $\frac{d[M]}{dt} = -kp[M][R^{\cdot}] - kp[M][P^{\cdot}]$ $\frac{d[P^{\cdot}]}{dt} = kp[M][R^{\cdot}] - 2kt[P^{\cdot}] - ko[O_2][P^{\cdot}]$ $\frac{d[O_2]}{dt} = -\mathrm{ko}[P^{\cdot}][O_2]$	Species balance during photopolymerization process in resin domain

TABLE VII. REACTION CONSTANTS FOR RESIN CURING PROCESS

Parameter	Value	Description
I_o	3.5mWcm^{-2}	Light intensity [46]
β	7e-4 cm^2 /mW·s	Photoinitiation coefficient [54]
kp	0.6 m^3/ mol·s	Propagation coefficient [56]
k_o	70 m^3/ mol·s	Oxygen inhibition coefficient [41]
k_t	1000 m^3/ mol·s	Self-termination coefficient [56]

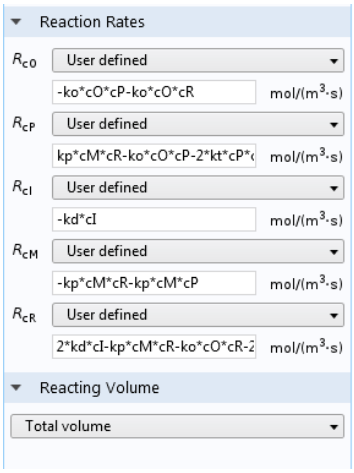

Figure 20. Photopolymerization reactions in resin domain.

During oxygen transportation route in Figure 19 green arrow shows, the diffusion of oxygen was assumed to start from PDMS to resin due to concentration gradient. Oxygen inside acrylic domain was neglected as the oxygen permeation of acrylic is three orders less than that of PDMS [25, 39, 57]. Stiff-spring continuous flux boundary conditions was applied on boundaries Y (y1,y2 in Figure 19) because of the discontinuities of oxygen concentration [58]. To obtain continuous fluxes over the boundaries, stiff-spring method was applied using the following equations:

$$N_0 = \mathrm{M}\left|C_{o2,j+1} - K_j C_{o2,j}\right| \tag{3.2}$$

$$K_j = \frac{C^e_{o2,j+1}}{C^e_{o2,j}} \tag{3.3}$$

where j denotes air, PDMS and resin domains, separately. M represents a large constant which keeps the term within absolute values zero. $C_{o2,j}$ means the oxygen concentration in different domains, $C^e_{o2,j}$ means the equilibrium oxygen concentration in different domains. K_j is derived from Henry's Law, and it is a dimensionless partition coefficient that can be calculated via equation 3.2 [59].

3.3.3 Meshing

Numerical solutions for the mathematics model were analyzed using COMSOL Multiphysics based on grid meshing and error control with variety of numerical solvers [60]. Generally, COMSOL generates mesh in triangular shape. However, we adopted mapped mesh for the resin domain of the finite element model to obtain a smoother oxygen concentration distribution (Figure 21).

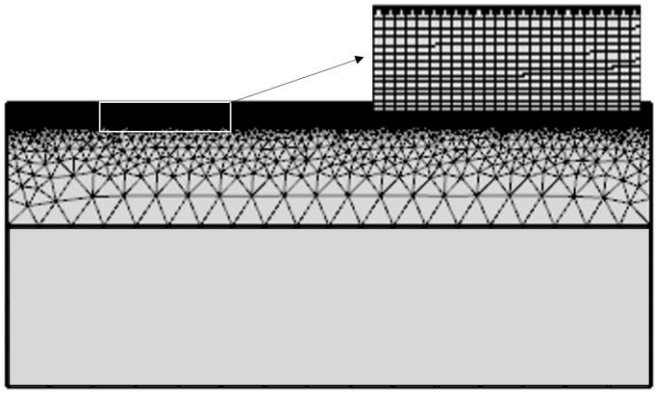

Figure 21. Finite element model used in COMSOL.

3.4 Photopolymerization validation

Photopolymerization experiments were performed on our CSVP system to validate the model described in this Chapter (experimental details will be discussed in next Chapter), polymerized parts were cured on the vat, and removed afterwards. A conventional caliper was used to measure the height of cured parts. The CSVP system includes an imaging unit (DLP LightCrafter 4500TM) and a resin vat. A digital mask planning testbed integrated with geometry slicing and motion controlling module was developed by C++ using Microsoft Visual Studio software. EnvisionTEC LS 600M acrylic resin was used in experimental test, and projection time

used is 6s, 12s, 18s, 24s, respectively. The photopolymerization can be validated by comparison of the height of cured part in experiment and the height of cured part in simulation.

The height of cured part is estimated according to the monomer conversion limit in chapter 2.3. Since the part profile can be estimated by tracking the monomer that reached the conversion limit, thus the part height can be obtained. With model created in last section, the part height at 6s, 12s, 18s, 24s are obtained in simulation, the results are shown in Figure 13, the blue parts.

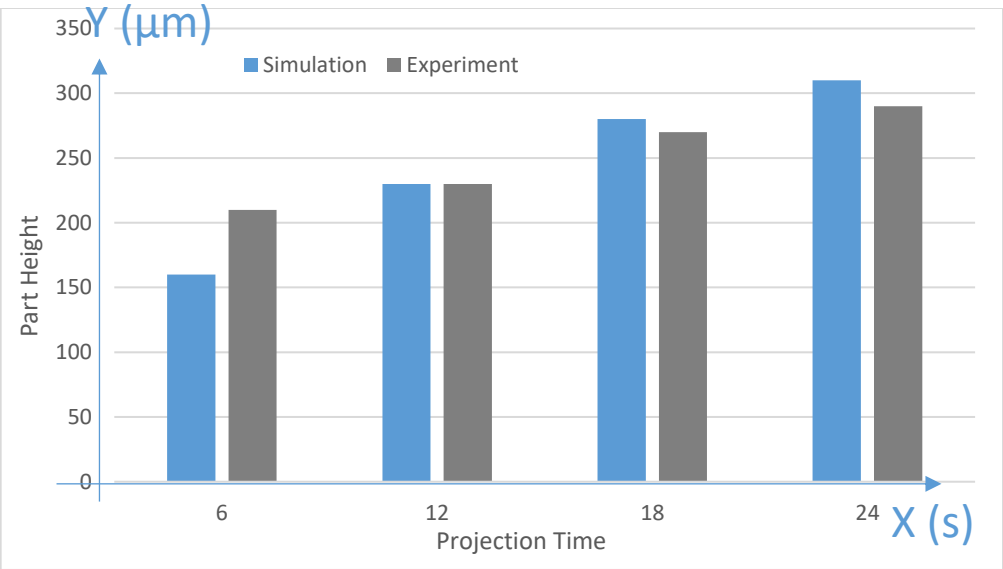

Figure 22. Comparison of predicted height of cured part from simulation and experimental results.

Figure 22 shows the comparison of the predicted height of cured part generated from COMSOL simulation and experiment, the x axis represents the curing time in second, and the y-axis represents the cured part height in μm. This result indicates that the photopolymerization mechanism and the parameters and physics used in this model is coincident with the experiment.

3.5 Oxygen inhibition illustration

To show how the oxygen inhibition works better, the rate constants of photopolymerization reaction are adjusted to decrease the curing speed, which indicated some clearer results for oxygen inhibits polymerization.

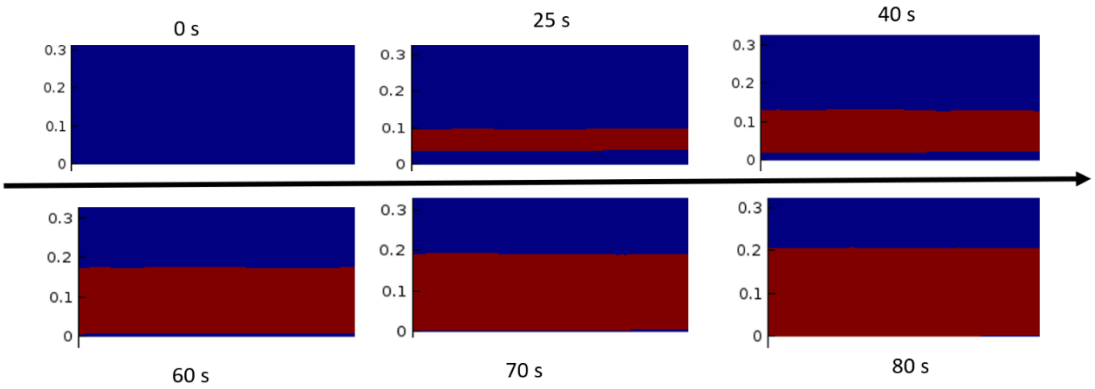

Figure 23. Scheme of curing process.

In Figure 23, the red domain denotes the cured part while blue one denotes the uncured resin. Here, the contour of cured part was estimated by tracking the coordinates where the monomer conversion has reached 12% (the critical conversion limit in the resin) [44]. Moreover, y axis in Figure 22 represents the thickness of resin. It is worth noting that the curing part becomes larger along with the time passes. A clear blue domain that indicates the oxygen inhibition layer is formed when the curing process undergoes for 25 seconds. However, the thickness of the oxygen inhibition layer decreases afterwards, which can be attributed to rapid oxygen consumption and insufficient supply from diffusion. As aforementioned, as the uncured resin that lies between the cured parts and the surface of the vat works as a lubrication layer, the separation force undoubtedly can be reduced significantly.

3.6 Summary

This chapter introduces the modeling process, boundary conditions and physics mechanisms applied for the simulation of the resin curing process. From experiment, the LS600M resin with thickness of around 200 μm is cured in 6s, the model built on the specified boundary conditions and parameters is validated by this curing speed. Oxygen inhibition using the proposed model was shown to be successful, and it was validated to have the capability of reducing the separation force by forming a lubrication layer where the resin cannot be cured.

Chapter 4 Study of effect of air-diffusion-channel on separation force

To further study the effect of oxygen inhibition capability from PDMS layer on the separation force during a long printing process, experiments have been conducted to record the separation force trending when printing a part with height of 20 mm within 1000s using two different vats: the vat of conventional design and vat with air-diffusion-channel [31]. It has indicated that the design with air-diffusion-channel resulted in the reduction of separation force. In this thesis, we further conducted the simulations on the trend of the oxygen concentration of the inhibition layer using different vats, giving rise to the analysis of the relationship between oxygen concentration and the separation force.

4.1 Mechanism simplification

In a regular CSVP printing process, a thin layer of the liquid photosensitive polymer is solidified on the platform upon the irradiation of light sources such as digital light processing (DLP) projector or laser beam etc. [61, 62]. Then the platform moves up, and the gap between cured part and the constraint surface of vat is refilled with fresh resin. A whole 3D printing process is completed by repeating the resin curing and platform pulling-up steps. In the last chapter, we have validated our model of the photopolymerization in the resin curing step. To study the effect of air-diffusion channel on separation force, we converted it to study the effect of oxygen concentration on separation force. The oxygen comes from the resin, PDMS itself and the diffused oxygen from atmosphere by air-diffusion channel as shown in Figure 24 and is consumed by reacting with polymer in photopolymerization. As same as the last model, the oxygen transportation from acrylic substrate is neglected since its lower oxygen permeability.

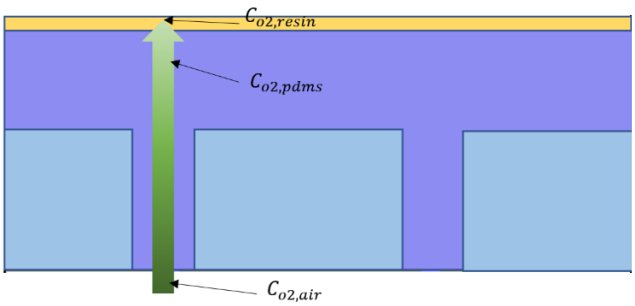

Figure 24. Oxygen transportation route.

To focus on the oxygen concentration in the whole printing process, considering that the oxygen is mainly consumed by polymer, we simplified the mechanism validated in last chapter to equation 4.1:

$$\frac{d[O_2]}{dt} = -\mathrm{ko}[P^{\cdot}][O_2] + D_{O_2}\{\frac{\partial^2[\mathrm{O_2}]}{\partial \mathrm{x}^2} + \frac{\partial^2[\mathrm{O_2}]}{\partial \mathrm{z}^2}\} \tag{4.1}$$

4.2 Modeling process

The modeling process of this section is similar to the last one, geometry modeling, physics definition and meshing parts are included, but the details of these parts are different.

4.2.1 Geometry modeling

A two-dimensional (2D) model was created to simulate the oxygen permeation and photopolymerization process. It is composed of three domains: the acrylic, PDMS (oxygen feed side) and resin (polymerization reaction zone) domains (Figure 25).

The geometry dimension of this model is same as the one in chapter 3 except the dimension of the air-diffusion channel (TABLE VIII). As we said in chapter 3, this 2D model represents a part cross-section of the real tank. To reflect the real effect of air-diffusion channel, the ratio of area of channel to the tank surface area is converted to the ratio of width of the two

grooves to the width of tank to better simulate the effect of air-diffusion channel. For this thesis, the ratio from 0% to 67% is considered, that means the wid_groove changes from 0mm to 4mm.

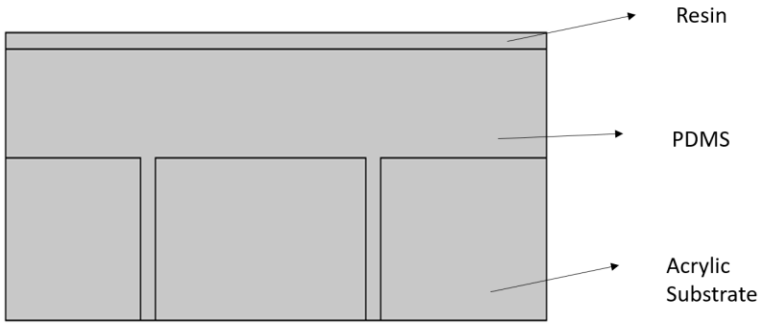

Figure 25. Geometry model with air-diffusion channel.

TABLE VIII. PARAMETERS PRESET IN GLOABLE DEFINITION

Parameter	Value	Description
th_pdms	2[mm]	Thickness of PDMS
wid_pdms	12[mm]	Width of PDMS
th_resin	0.3[mm]	Thickness of resin
wid_groove	0.5[mm]	Width of groove
th_acrylic	3[mm]	Thickness of acrylic substrate

4.2.2 Physics module

It should be noticed that as the consumed photoinitiators and monomers in the gap between cured part and vat substrate are always replenished by fresh resin during the fabrication process, a dynamic species balance is formed. For long-term process, we assume that the radical species concentration in the gap remain constant while the oxygen keeps decreasing.

In order to calculate the dynamic concentration during a long-term process, we first obtained the equilibrium concentration of photoinitiators and monomers from resin curing step based on the model in chapter 3.

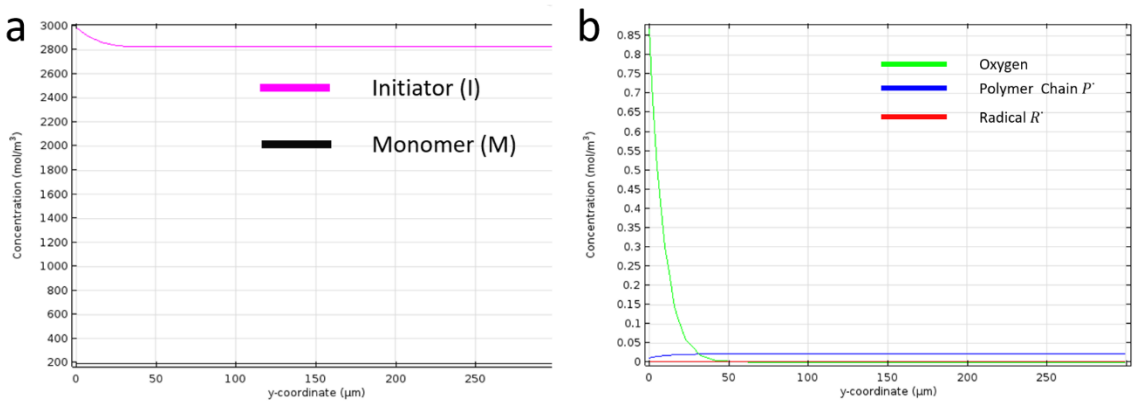

Figure 26. a) Concentration of Initiator and Monomer in the first cured layer. b) Concentration of Oxygen and Polymer chain (P·) in the first cured layer.

Figure 26 illustrates the species concentration distribution along the thickness of resin after the first layer is cured. Considering the fact that after the first layer is cured, the gap (the thickness of gap is 250 μm normally) can be refilled by fresh resin, the concentration of the reactants will change. Thus, we defined the average value of the concentration reactants in the oxygen inhibition layer (within the thickness of 50 μm) as shown in TABLE IX as the dynamically balanced concentration in the long-term process.

TABLE IX. SPECIES CONCENTRATION FOR ENTIRE PRINTING PROCESS

Parameters	**Value**	**Description**
$C_{o2,pdms}$	2.8 mol/m^3	Oxygen concentration in PDMS
$C_{o2,resin}$	0.5 mol/m^3	Oxygen concentration in resin
C_I	193 mol/m^3	Photoinitiator concentration in resin
C_M	2883 mol/m^3	Monomer concentration in resin
C_P	0.024 mol/m^3	Polymer concentration in resin

Since only oxygen and polymer are needed based on the simplified mechanism in the physics interface, the concentration of oxygen in PDMS and resin and the polymer concentration are used as initials in PDMS and resin physics.

Oxygen transportation and oxygen consuming reaction (TABLE XII) are coupled in this model. As we pointed out previously in section 4.1, the mechanism is simplified to equation 4.1. The boundary conditions of PDMS and resin and the domain physics of resin (as shown in TABLE X and XI) are defined based on the oxygen transport process and the equation 4.1.

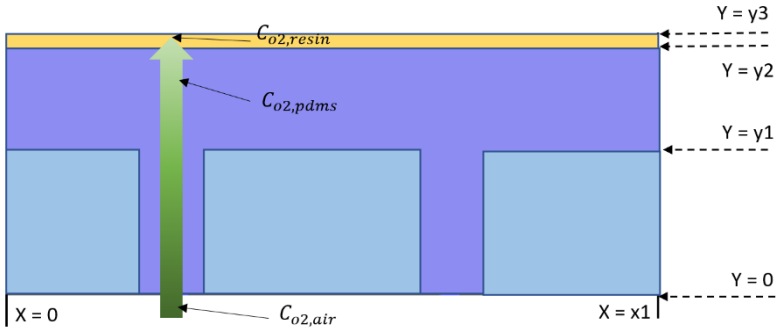

Figure 27. Domains and boundaries used in the model and oxygen transportation.

TABLE X. BOUNDARY CONDITIONS OF PDMS DOMAIN

Boundary Conditions	**Description**
-n·N=M$\lvert C_{o2,pdms} - K_1 C_{o2,air} \rvert$	@Y=0, Stiff-spring Continuous Flux
n·N=0	@Y=y1, Insulation
-n·$N_{src} = n{\cdot}N_{dst}$	@X=0, X = x1, Periodic Condition

TABLE XI. BOUNDARY CONDITIONS OF RESIN DOMAIN

Boundary Conditions	**Description**
-n·N=M$\lvert C_{o2,resin} - K_2 C_{o2,pdms} \rvert$	@Y=y2, Stiff-spring Continuous Flux
n·N=0	@Y= y3, Insulation
-n·$N_{src} = n{\cdot}N_{dst}$	@X=0, X= x1, Periodic Condition

TABLE XII. REACTIONS IN RESIN DOMAIN

Reactions	**Description**
$\frac{d[O_2]}{dt} = -\mathrm{ko}[P^{\cdot}][O_2]$	Oxygen consumption reaction

4.2.3 Meshing

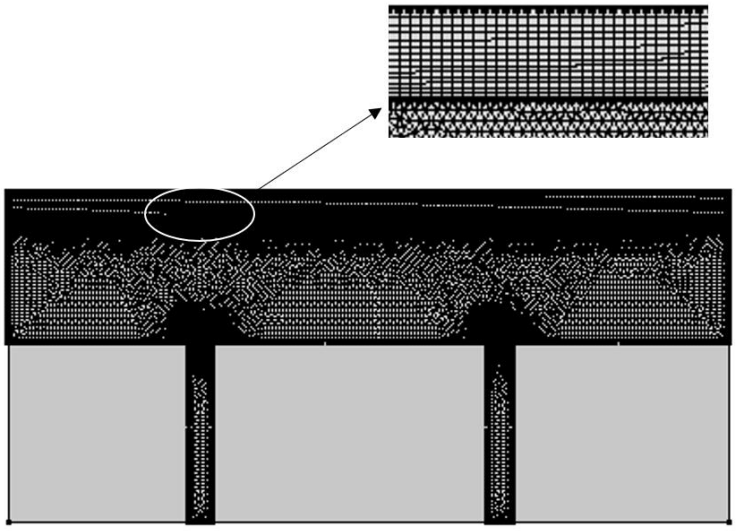

Figure 28. Mapped mesh of air-diffusion channel design.

As same as the model created in chapter 3, mapped mesh for the resin domain of the finite element model is adapted to obtain a smoother oxygen concentration distribution (Figure 28).

4.3 Estimation of effective printing time

Since the simulation model only reflect the trending of oxygen concentration during the printing process, how to connect this with separation force is a problem. To address this, a definition called effective printing time is proposed in this thesis. An effective printing time means during this printing period, the separation force is not large enough to produce bad effect neither on PDMS nor on cured part.

Figure 29 shows a simulation result of the 3% area ratio of air-diffusion channel to tank surface. The y axis is oxygen concentration in the gap, x axis is time, the result illustrates that the oxygen concentration in the gap decreases along with the printing going.

To obtain the effective printing times from the oxygen concentration results, a critical value of oxygen concentration 0.15 mol/m^3 was used, owing to the fact that when the oxygen concentration exceeds this value, the majority of the resin has reached the critical monomer conversion limit. It also indicates that the oxygen inhibition layer depletes, hence the separation force increases from this point. Therefore, the time that oxygen concentration exceeds concentration 0.15 mol/m^3 is considered as effective printing time. Thus, from Figure 28 we can read that the effective printing time for 3% channel area ratio tank is about 1150s.

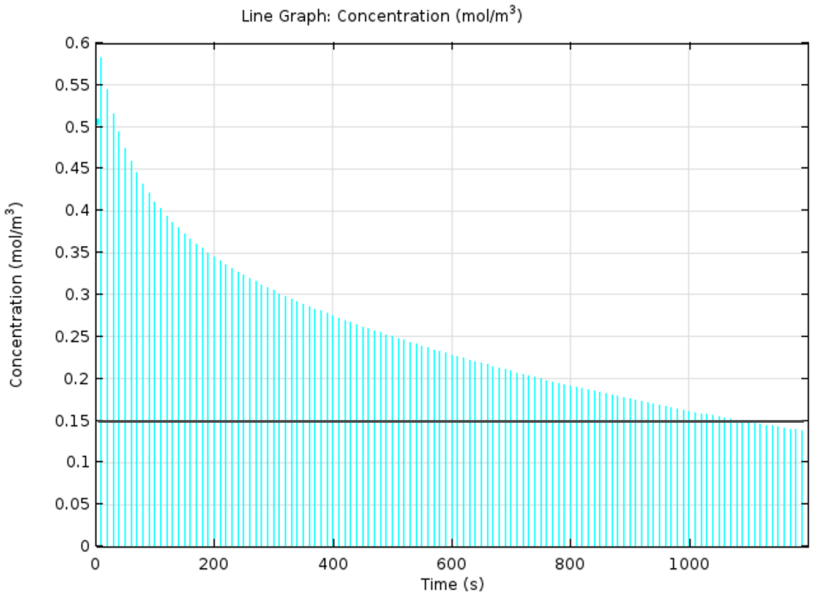

Figure 29. Oxygen concentration changed during printing process in 3% channel area ratio tank.

4.4 Validation

One experiment was conducted in [31] to test the effort of oxygen inhibition layer on separation force. A 20mm tall object was printed in resin vat, Separation force values were recorded during the printing process. For the conventional constraint surface, during the printing process, the separation forces remain below 5N until about 900s increasing to 20N, while the separation force of new design maintains under 5N (Figure 30). This phenomenon denotes that when the oxygen concentration vicinity of the PDMS surface was decreased, separation force will increase greatly, which leads to a common 3D printing failure, layer adhesion failure. To avoid this failure, compensate oxygen consumption, control separation force, using oxygen permeable film as constraint surface and keep it contact with air directly was supposed [36, 63]. However, this method easily produces tensioning challenge and creases problem of film. Based on the conventional PDMS coating method, the new design air-diffusion-channel improved can work effectively offer oxygen and without leading to crease of film[31, 40].

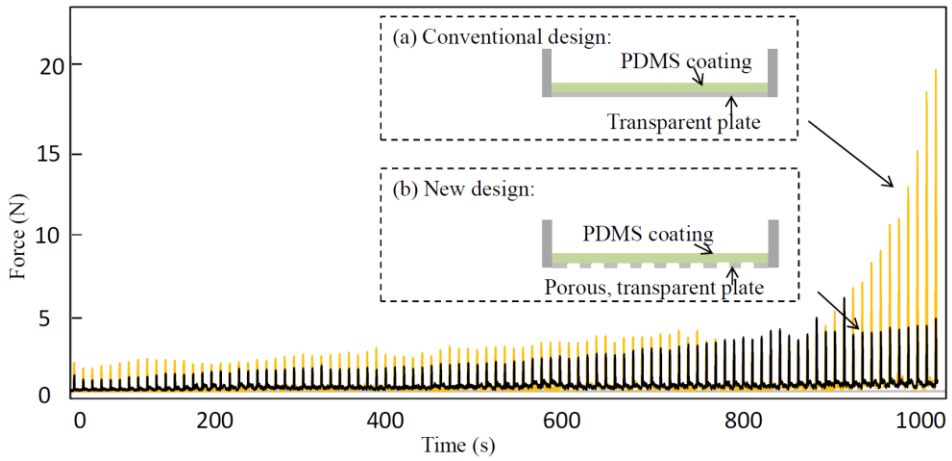

Figure 30. Separation forces in the process of printing a 20 mm tall solid cylinder with conventional method and new method. Adapted from [31].

Figure 31 illustrates how oxygen concentration changes along with the printing process, the red curve is the trending of conventional design, the cyan curve represents the trending of new design (using the model in Figure 32), compared with the critical oxygen concentration limit (black line), Figure 31 is coincident with Figure 30, around 900s, the oxygen concentration is lower than the limit, for the conventional design separation force increases sharply from 5N to 20N, while the new design can retain at low level separation force until 1000s. This result verifies that the oxygen-diffusion-channel facilitate the decreasing of separation force, can maintain the force in a lower level.

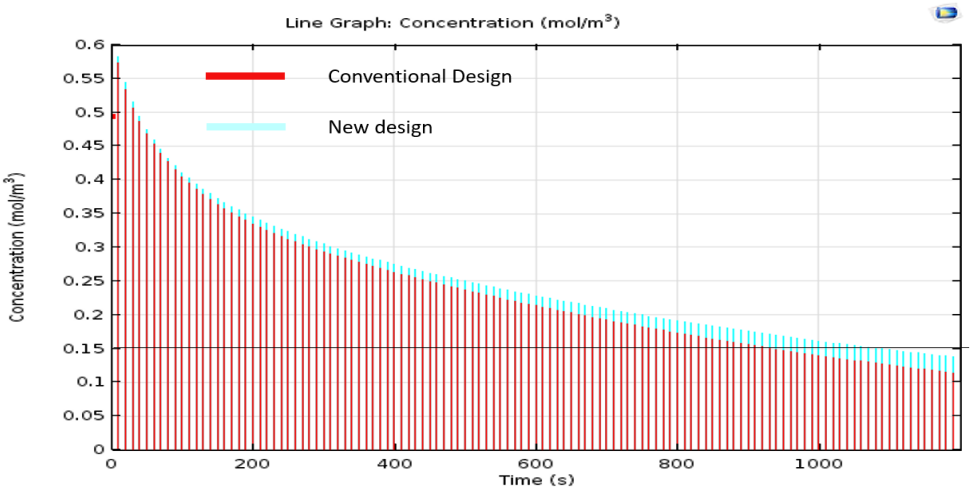

Figure 31. Oxygen Concentrations in the Printing Process with Conventional Method (Red Curve) and New Design (Cyan Curve).

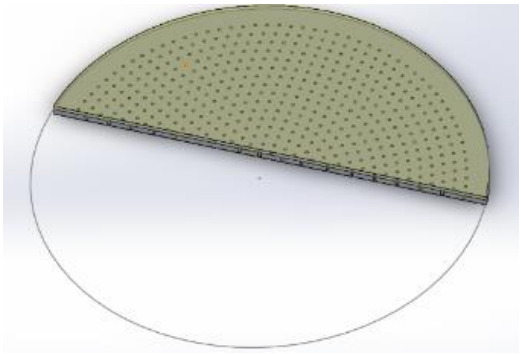

Figure 32. Constraint surface with air-diffusion-channel.

4.5 Experiment setup

A constrained surface stereolithography setup is built for separation force study, which includes imaging unit, resin vat, a linear actuator used to lift build platform, control unit and load cell. There are two types of resin vat, one is conventional design with normal constraint surface coating with PDMS, and another one is the new design with air-diffusion-channel constraint surface.

A digital mask planning testbed integrating with geometry slicing and motion controlling module was developed by C++ and Microsoft Visual Studio software. The testbed also can control

image projection with Z movements. An online separation force monitoring testbed was built in MATLAB to read and process data from the load cell, record real time changing separation force values.

Perfactory TM LS600M (yellow) from EnvisionTEC Inc. (Ferndale, MI) was used in experimental test; projection time is 45s, tanks with and without air-diffusion-channel to substrate surface are made to verify the effect of air-diffusion-channel to separation force (Figure 33).

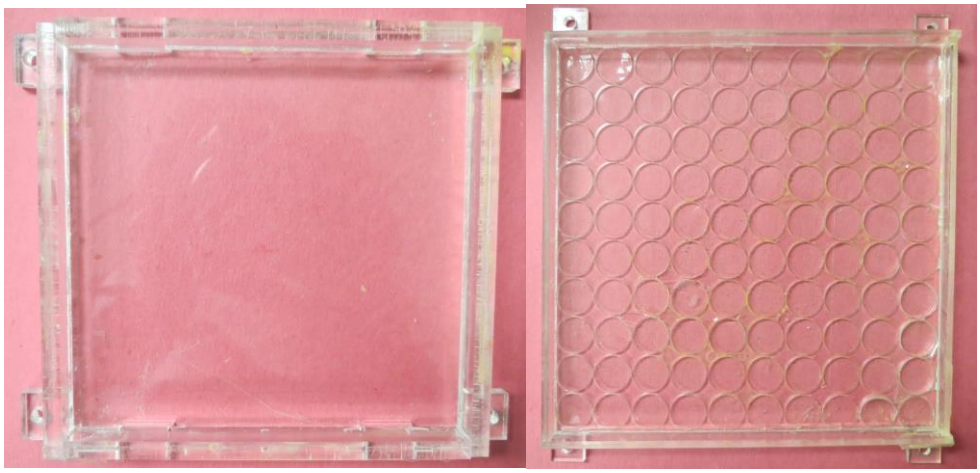

Figure 33. Tanks with and without oxygen-diffusion-channel used in experiments.

4.6 Results and discussion

The last section introduces the benefit of the oxygen-diffusion-channel, and validates the model employed for the simulation. Considering only the conventional tank and the 3% channels tank (Figure 15) are hired in the paper [31], the relationship between the effective printing time and the area ratio of oxygen-diffusion-channel is worth to study. In the simulations for the tanks with different area ratio of oxygen-diffusion-channel, only oxygen diffusion and photopolymerization are incorporated, the effective printing time which can be obtained from the results like Figure 30 for different tanks follow the below curve in Figure 34.

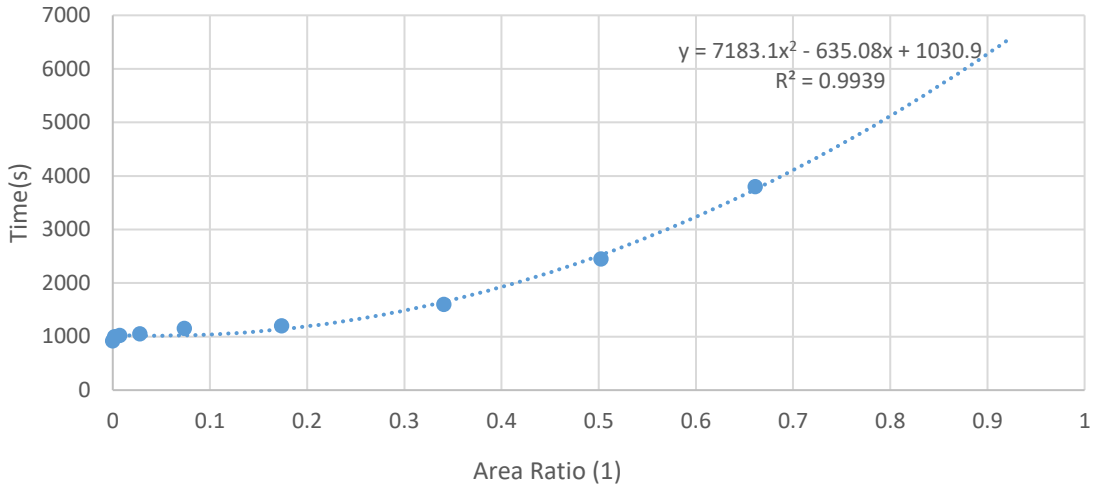

Figure 34. Effect of channel area ratio to effective printing time.

Figure 34 predicts that effective printing time increases along with the increase of area ratio of air-diffusion-channels to surface. It also manifests that the separation force can be maintained at a low level, giving rise to an easier fabrication process. The blue dashed curve is an approximation line by applying the fitted equation $y = 7183.1x^2 - 635.08x + 1030.9$, where y is the effective printing time, x is the ratio of channels area to surface area.

Nevertheless, the trending in Figure 34 can only be considered as effective when the area ratio is below 67%. This can be ascribed to sufficient oxygen supply from highly oxygen permeability from PDMS, which compensates the consumption from reactions (Figure 35).

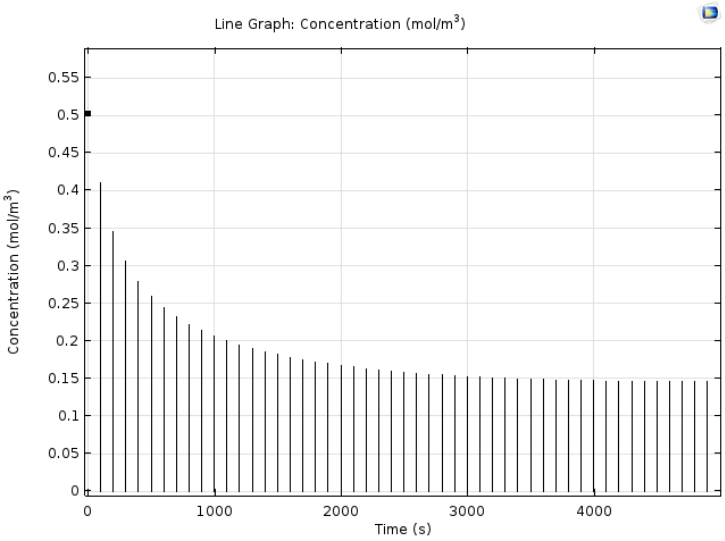

Figure 35. Oxygen Concentrations in Printing Process

To validate the result further, a tank with 0%, 3%, 67% channels and a tank without oxygen-diffusion-channel are used to repeat the experiment in [31], the separation forces in the printing process shows in Figure 36, 36 and 37.

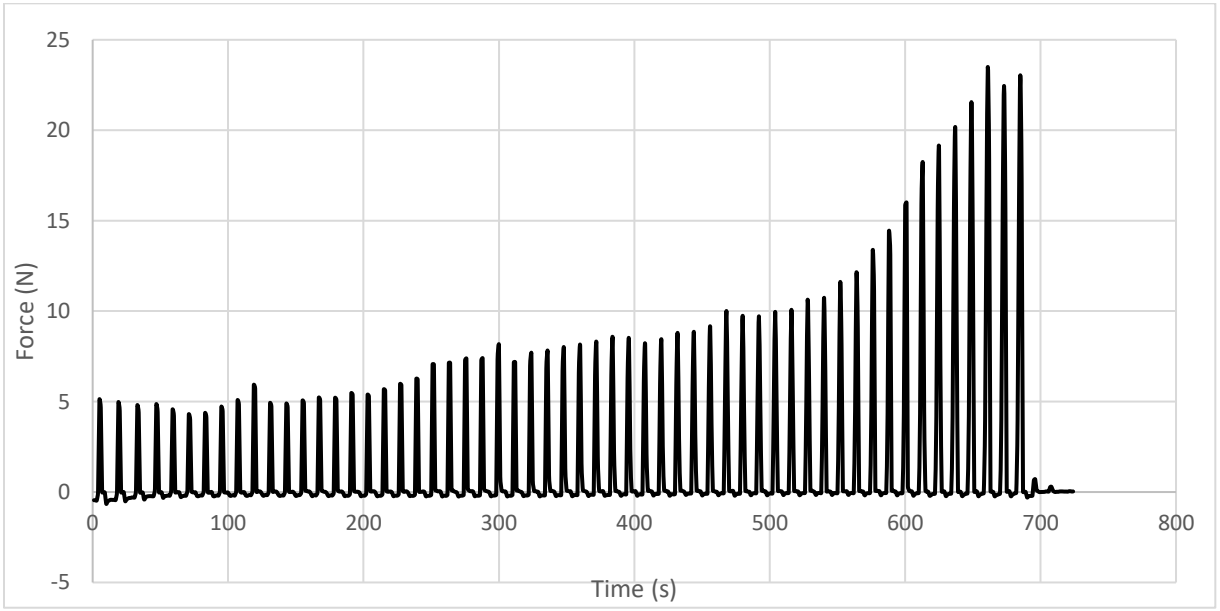

Figure 36. Separation force in the printing process for conventional design tank.

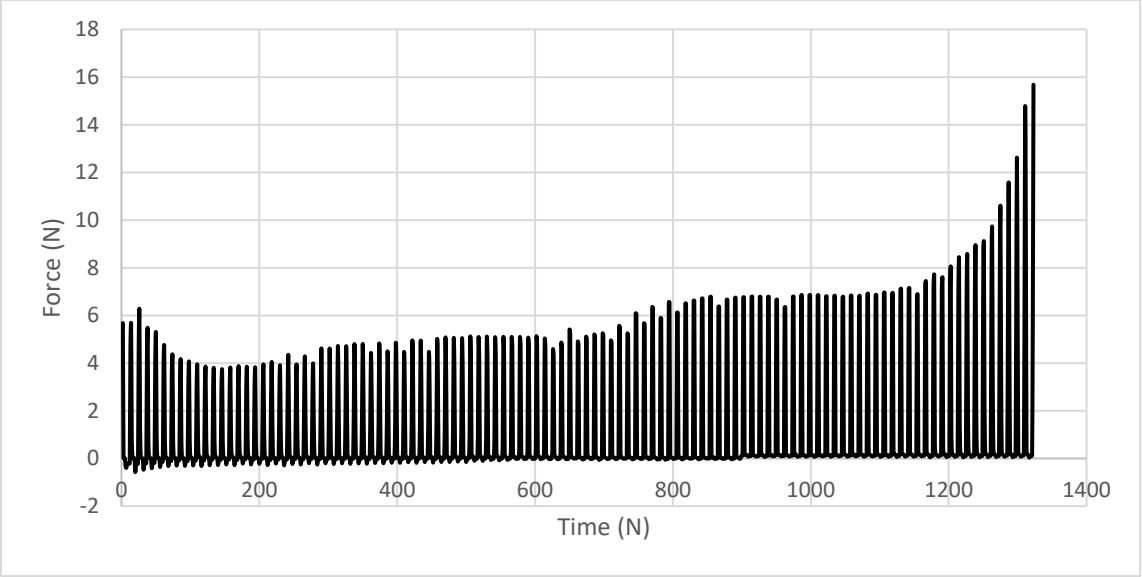

Figure 37. Separation force in the printing process for 3% channels tank.

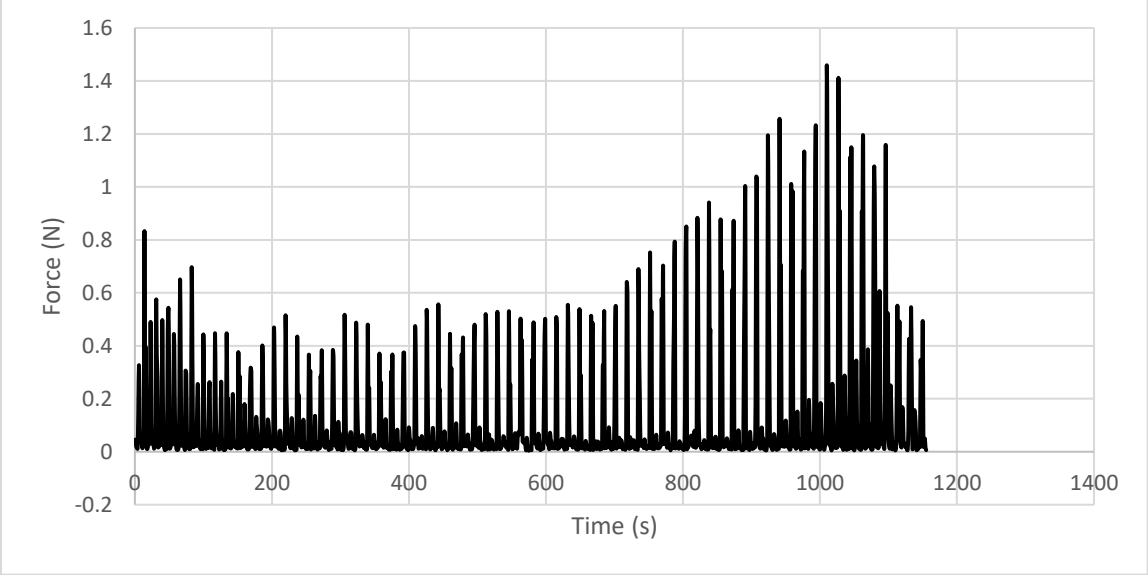

Figure 38. Separation force in the printing process for 67% channels tank.

The Y-axis is the separation force value, while the X-axis is printing time in Figure 36 to Figure 38. In the Figure 20, where the separation force increased greatly from 5N to 24 N around 700s like the Figure 29 in the paper [31], the separation force in Figure 37 increase to 16 N in 1300s; but it can be noticed that in the Figure 38 the force values are maintained under 1.7N during the whole process which is far less than the 24N, the maximum value produced in the

conventional design tank. This decrease in separation force from 24N to 1.7N proves the effect of oxygen-diffusion-channel on separation force, since the larger area ratio of channels will supply sufficient oxygen to the oxygen inhibition layer.

From the Figure 39, it is obvious that the curing degree are different between the resin above the channel and the resin above the non-porous substrate, thus we propose that the difference of optical property of acrylic substrate and the PDMS, or the lower oxygen concentration above the un-porous PDMS makes the non-uniform separation force distributed on the cross section that lead to the printing process in Figure 39 failed around 1200s not continued as the simulation result shows. Even though the part failed around 1200s, but the pretty low separation force can be used to prove that under ideal condition if only oxygen is considered the printing process can be last in a long time as the simulation predicts.

Figure 39. Cured part in 67% channel tank

4.7 Summary

The oxygen inhibition layer is affected by judicious selection of control parameters, such as the photon flux, resin optical and curing properties[36]. From the photopolymerization

reactions, we can realize that the concentration of [PI] and light intensity would decrease the thickness of un-cross-linked layer by consuming oxygen, while the sufficient oxygen supply will enhance the oxygen inhibition layer. In this chapter, following the verified parameter such as photoinitiation concentration, initial oxygen concentration in resin and PDMS, light intensity etc. and the simplified mechanism for long-term printing process, a model which concerns the effect of oxygen-diffusion-channel on separation force is built. The model is validated by compared to the experiment in [31], which prove that the oxygen-diffusion-channel can realize the objective of decrease separation force by supply oxygen from aerated atmosphere. To study the effect furthermore and get the optimum structure, the simulations and experiments for different area ratio tanks are set up, the results show that the sufficient oxygen can maintain the separation force at a low level and the relationship of the effective printing time and the area ratio under 67% follows the fitted equation $y = 7183.1x^2 - 635.08x + 1030.9$.

Chapter 5 Conclusion and Future Work

To conclude, we conducted the simulation of using air-diffusion-channel constrained surfaces towards reducing large separation force during constrained surface vat photopolymerization fabrication process and the impact of imparting oxygen inhibition layer by means of using oxygen-permeable material (PDMS). Specifically, a thin layer of PDMS is added to the porous acrylic surface, thereby continuous oxygen supply is obtained owing to high oxygen permeability through PDMS. Therefore, different from conventional constrained surface vat photopolymerization, a thin layer where polymerization is inhibited continuously by oxygen can be maintained during fabrication process, hence acting as a lubricant layer for reducing the separation force.

In this study, the photopolymerization and oxygen transportation process have been investigated. Typically, photopolymerization includes initiation, propagation, termination and oxygen inhibition stages, and the main reactions behind were introduced in Chapter 2. Moreover, we also described and discussed the polymerization rate, critical conversion limit which are important for the quantification of the curing degree [44].

In Chapter 3, the software COMSOL and the module 'Transport of Diluted Species' were described and applied for the simulation of resin curing process. The photopolymerization reactions were also coupled in the module. Based on the mechanism introduced in Chapter 2, we configured the setup for the modeling process such as the initial parameters and boundary conditions, which were also validated by the curing speed obtained in the experiments. Lastly, we also showed how the oxygen inhibition layer was formed (Chapter 3).

Additionally, we supposed that oxygen-diffusion-channels of a new design were responsible for un-cross-linked layer above the tank surface in a long-term printing process. Moreover, it was found that the oxygen-diffusion-channel had the ability to enhance the oxygen inhibition for reducing the separation force and prolong the effective printing time. The relationships of ratio of air-channel area to the surface area and effective printing time have been explored via experiments and simulations. It was shown that when the area ratio was below 67%, the relationship showed a good agreement with the approximate curve. While the separation force for the tank with a ratio of 67% maintained at a very low level and reached the expectation, the fabrication of the part failed before the simulation time was over.

For the future work, the reasons caused the printing failure for the tank with the ratio of 67% should be addressed. The optical property of acrylic substrate and PDMS, and the adhesion property of PDMS should also be considered. Since the parameters of concentration of monomer and initiator and the rate constant were estimated and obtained from other papers but experiments, which may lead to the inaccuracy of our results. To fix this drawback, we will try to obtain the oxygen diffusion constants in the PDMS and resin, accurate reaction rates of the photopolymerization, and other parameters by using homemade photosensitive materials with known recipe rather than using commercial ones.

Cited Literature

1. Huang, S.H., et al., *Additive manufacturing and its societal impact: a literature review.* The International Journal of Advanced Manufacturing Technology, 2013. **67**(5-8): p. 1191-1203.
2. Rayna, T. and L. Striukova, *From rapid prototyping to home fabrication: How 3D printing is changing business model innovation.* Technological Forecasting and Social Change, 2016. **102**: p. 214-224.
3. Standard, A., *ISO/ASTM 52900: 2015 Additive manufacturing-General principles-terminology.* ASTM F2792-10e1, 2012.
4. Bogue, R., *3D printing: the dawn of a new era in manufacturing?* Assembly Automation, 2013. **33**(4): p. 307-311.
5. Mikołajewska, E., et al., *3D printing technologies in rehabilitation engineering.* 2014.
6. Minas, C., et al., *3D printing of emulsions and foams into hierarchical porous ceramics.* Advanced Materials, 2016. **28**(45): p. 9993-9999.
7. Chia, H.N. and B.M. Wu, *Recent advances in 3D printing of biomaterials.* Journal of biological engineering, 2015. **9**(1): p. 4.
8. Carrico, J.D., et al., *Fused filament 3D printing of ionic polymer-metal composites (IPMCs).* Smart Materials and Structures, 2015. **24**(12): p. 125021.
9. Gibson, I., D. Rosen, and B. Stucker, *Additive manufacturing technologies, 3D printing, rapid prototyping, and direct digital manufacturing, Springer.* New York Heidelberg Dordrecht London, 2010.
10. Campbell, T., et al., *Could 3D printing change the world.* Technologies, Potential, and Implications of Additive Manufacturing, Atlantic Council, Washington, DC, 2011.

Cited Literature (Continued)

11. Bird, J., *Exploring the 3D printing opportunity.* The Financial Times. Retrieved, 2012: p. 08-30.

12. Hull, C.W., *Apparatus for production of three-dimensional objects by stereolithography*. 1986, Google Patents.

13. DeSimone, J.M., A. Ermoshkin, and E.T. Samulski, *Method and apparatus for three-dimensional fabrication*. 2016, Google Patents.

14. Derby, B., *Printing and prototyping of tissues and scaffolds.* Science, 2012. **338**(6109): p. 921-926.

15. Atala, A., F.K. Kasper, and A.G. Mikos, *Engineering complex tissues.* Science translational medicine, 2012. **4**(160): p. 160rv12-160rv12.

16. Gross, B.C., et al., *Evaluation of 3D printing and its potential impact on biotechnology and the chemical sciences*. 2014, ACS Publications.

17. Sun, K., et al., *3D printing of interdigitated Li-Ion microbattery architectures.* Advanced materials, 2013. **25**(33): p. 4539-4543.

18. Symes, M.D., et al., *Integrated 3D-printed reactionware for chemical synthesis and analysis.* Nature chemistry, 2012. **4**(5): p. 349.

19. Chakraborty, P. and R.N. Zuckermann, *Coarse-grained, foldable, physical model of the polypeptide chain.* Proceedings of the National Academy of Sciences, 2013. **110**(33): p. 13368-13373.

20. Kitson, P.J., et al., *Bringing crystal structures to reality by three-dimensional printing.* Crystal Growth & Design, 2014. **14**(6): p. 2720-2724.

Cited Literature (Continued)

21. Erkal, J.L., et al., *3D printed microfluidic devices with integrated versatile and reusable electrodes.* Lab on a Chip, 2014. **14**(12): p. 2023-2032.

22. Ikuta, K. and K. Hirowatari. *Real three dimensional micro fabrication using stereo lithography and metal molding*. in *Micro Electro Mechanical Systems, 1993, MEMS'93, Proceedings An Investigation of Micro Structures, Sensors, Actuators, Machines and Systems. IEEE.* 1993. IEEE.

23. Suzumori, K., A. Koga, and H. Riyoko. *Microfabrication of integrated FMAs using stereo lithography*. in *Micro Electro Mechanical Systems, 1994, MEMS'94, Proceedings, IEEE Workshop on*. 1994. IEEE.

24. Takagi, T. and N. Nakajima. *Architecture combination by micro photoforming process*. in *Micro Electro Mechanical Systems, 1994, MEMS'94, Proceedings, IEEE Workshop on*. 1994. IEEE.

25. Pan, Y., C. Zhou, and Y. Chen, *A fast mask projection stereolithography process for fabricating digital models in minutes.* Journal of Manufacturing Science and Engineering, 2012. **134**(5): p. 051011.

26. Wallace, J., et al., *Validating continuous digital light processing (cDLP) additive manufacturing accuracy and tissue engineering utility of a dye-initiator package.* Biofabrication, 2014. **6**(1): p. 015003.

27. Sun, H.-B., et al., *Experimental investigation of single voxels for laser nanofabrication via two-photon photopolymerization.* Applied physics letters, 2003. **83**(5): p. 819-821.

28. Kawata, S., et al., *Finer features for functional microdevices.* Nature, 2001. **412**(6848): p. 697.

Cited Literature (Continued)

29. Serbin, J., et al., *Femtosecond laser-induced two-photon polymerization of inorganic–organic hybrid materials for applications in photonics.* Optics letters, 2003. **28**(5): p. 301-303.

30. Liravi, F., S. Das, and C. Zhou, *Separation force analysis and prediction based on cohesive element model for constrained-surface Stereolithography processes.* Computer-Aided Design, 2015. **69**: p. 134-142.

31. Pan, Y., et al., *Study of separation force in constrained surface projection stereolithography.* Rapid Prototyping Journal, 2017. **23**(2): p. 353-361.

32. Chen, Y., C. Zhou, and J. Lao, *A layerless additive manufacturing process based on CNC accumulation.* Rapid Prototyping Journal, 2011. **17**(3): p. 218-227.

33. Huang, Y.-M. and C.-P. Jiang, *On-line force monitoring of platform ascending rapid prototyping system.* Journal of materials processing technology, 2005. **159**(2): p. 257-264.

34. Zhou, C., et al. *Development of multi-material mask-image-projection-based stereolithography for the fabrication of digital materials*. in *Annual solid freeform fabrication symposium, Austin, TX*. 2011.

35. Pan, Y., C. Zhou, and Y. Chen, *A Fast Mask Projection Stereolithography Process for Fabricating Digital Models in Minutes.* Journal of Manufacturing Science and Engineering, 2012. **134**(5): p. 051011-051011-9.

36. Tumbleston, J.R., et al., *Continuous liquid interface production of 3D objects.* Science, 2015: p. aaa2397.

37. Pan, Y., et al., *Smooth surface fabrication in mask projection based stereolithography.* Journal of Manufacturing Processes, 2012. **14**(4): p. 460-470.

Cited Literature (Continued)

38. Song, X., et al., *Ceramic fabrication using mask-image-projection-based stereolithography integrated with tape-casting.* Journal of Manufacturing Processes, 2015. **20**: p. 456-464.

39. Pan, Y., Y. Chen, and Z. Yu, *Fast mask image projection-based micro-stereolithography process for complex geometry.* Journal of Micro and Nano-Manufacturing, 2017. **5**(1): p. 014501.

40. He, H., et al., *Air-Diffusion-Channel Constrained Surface Based Stereolithography for Three-Dimensional Printing of Objects With Wide Solid Cross Sections.* Journal of Manufacturing Science and Engineering, 2018. **140**(6): p. 061011.

41. Odian, G., *Principle of polymerization. Hoboken*. 2004, NJ: John Wiley & Sons, Inc.

42. Cai, Y. and J.L. Jessop, *Decreased oxygen inhibition in photopolymerized acrylate/epoxide hybrid polymer coatings as demonstrated by Raman spectroscopy.* Polymer, 2006. **47**(19): p. 6560-6566.

43. Decker, C., *Photoinitiated curing of multifunctional monomers.* Acta Polymerica, 1994. **45**(5): p. 333-347.

44. Boddapati, A., *Modeling cure depth during photopolymerization of multifunctional acrylates*. 2010, Georgia Institute of Technology.

45. Odian, G., *Principles of polymerization*. 2004: John Wiley & Sons.

46. Zhao, Z., et al., *Effects of oxygen on light activation in covalent adaptable network polymers.* Soft matter, 2015. **11**(30): p. 6134-6144.

47. Jariwala, A.S., et al., *Modeling effects of oxygen inhibition in mask-based stereolithography.* Rapid Prototyping Journal, 2011. **17**(3): p. 168-175.

Cited Literature (Continued)

48. Koleske, J.V., *Radiation curing of coatings*. 2002: ASTM international West Conshohocken, PA.

49. Fouassier, J.-P., *Photoinitiation, photopolymerization, and photocuring: fundamentals and applications*. 1995: Hanser.

50. He, H., et al., *Effect of Constrained Surface Texturing on Separation Force in Projection Stereolithography.* Journal of Manufacturing Science and Engineering, 2018. **140**(9): p. 091007.

51. Decker, C. and A.D. Jenkins, *Kinetic approach of oxygen inhibition in ultraviolet-and laser-induced polymerizations.* Macromolecules, 1985. **18**(6): p. 1241-1244.

52. Lian, Q., et al., *Oxygen-controlled bottom-up mask-projection stereolithography for ceramic 3D printing.* Ceramics International, 2017. **43**(17): p. 14956-14961.

53. Flory, P.J., *Molecular size distribution in three dimensional polymers. I. Gelation1.* Journal of the American Chemical Society, 1941. **63**(11): p. 3083-3090.

54. Zhao, Z., et al., *Effects of oxygen on interfacial strength of incremental forming of materials by photopolymerization.* Extreme Mechanics Letters, 2016. **9**: p. 108-118.

55. Taki, K., et al., *Oxygen concentration and conversion distributions in a layer-by-layer UV-cured film used as a simplified model of a 3D UV inkjet printing system.* Chemical Engineering Science, 2017. **158**: p. 569-579.

56. Goodner, M.D. and C.N. Bowman, *Development of a comprehensive free radical photopolymerization model incorporating heat and mass transfer effects in thick films.* Chemical Engineering Science, 2002. **57**(5): p. 887-900.

Cited Literature (Continued)

57. Liravi, F., S. Das, and C. Zhou. *Separation Force Analysis based on Cohesive Delamination Model for Bottom-up Stereolithography Using Finite Element Analysis*. 2014. Solid Freeform Fabrication Symposium.

58. Clark, W.M. *COMSOL multiphysics models for teaching chemical engineering fundamentals: absorption column models and illustration of the two-film theory of mass transfer*. in *COMSOL Conference, Boston*. 2008.

59. Ghadimi, A., et al., *Ternary gas permeation through a synthesized PDMS membrane: experimental and modeling.* Journal of Membrane Science, 2009. **344**(1-2): p. 225-236.

60. Hekmat, A., A.E. Amooghin, and M.K. Moraveji, *CFD simulation of gas–liquid flow behaviour in an air-lift reactor: determination of the optimum distance of the draft tube.* Simulation Modelling Practice and Theory, 2010. **18**(7): p. 927-945.

61. Melchels, F.P., J. Feijen, and D.W. Grijpma, *A review on stereolithography and its applications in biomedical engineering.* Biomaterials, 2010. **31**(24): p. 6121-6130.

62. Zhang, X., X. Jiang, and C. Sun, *Micro-stereolithography of polymeric and ceramic microstructures.* Sensors and Actuators A: Physical, 1999. **77**(2): p. 149-156.

63. Chu, C., G. Graf, and D.W. Rosen, *Design for additive manufacturing of cellular structures.* Computer-Aided Design and Applications, 2008. **5**(5): p. 686-696.

VITA

Education

University of Illinois at Chicago(UIC) – Chicago, IL Master of Industrial Engineering (Dec. 2018 Expected) GPA: 4.0/4.0

Beijing Information Science and Technology University (BISTU) - Beijing, China Master of Mechanical Engineering (Sept.2012 – May.2015) GPA: 3.20/4.0

Hebei University of Engineering (HBE) – Handan, China Bachelor of Mechanical Design, Manufacturing and Automation (Sept.2008 – July.2012) GPA:3.62/4.0

Research Experience

UIC Xu Microfluidics Lab *Research Assistant* Aug 2017 - Present

Fabricated microfluidic chips using high resolution 3D printing technology for mixing (two-photon polymerization)

Simulated photopolymerization process in constrained surface stereolithography 3D printer

Professional Experience

Pre-contracting Layout Engineer (June. 2015 – Feb. 2017)

Gebo Cermex (Subsidiary of Tetra Pak Group) – Beijing, China

Gathered technical information for projects by hands-on measuring or communicating with clients

Designed and optimizes PET/CAN/GLASS production line layout regarding to requirements from clients by CAD

Prepared proposals and cost estimations for sales to grow business and provides exceptional client service

Worked with internal departments (Marketing, Project managing, Sourcing, etc.) to ensure proposals competitive

Offered technical support to sales and project managers alongside client meetings

Programmed a plug-in module of AutoCAD by V-lisp and VBA for conveyor design process

Mechanical Design Engineer Intern (Sept.2013 – Jan. 2015)

BGS Industrials – Beijing, China

Assisted manufacturing and designing staff in ball screw pair design layout with critical GD&T

Developed CAD and CAPP design modules for ball screw pair in AutoCAD with V-lisp and VBA

Publication

Lin. Y, Gao C, etc. Soft Lithography based on photolithography and two-photon polymerization, Microfluidics and Nanofluicics

Software Copyright: BGS-CAD system of ball screw pair; BGS-CAPP system of ball screw pair.

Appendix

Permission for Figure 4

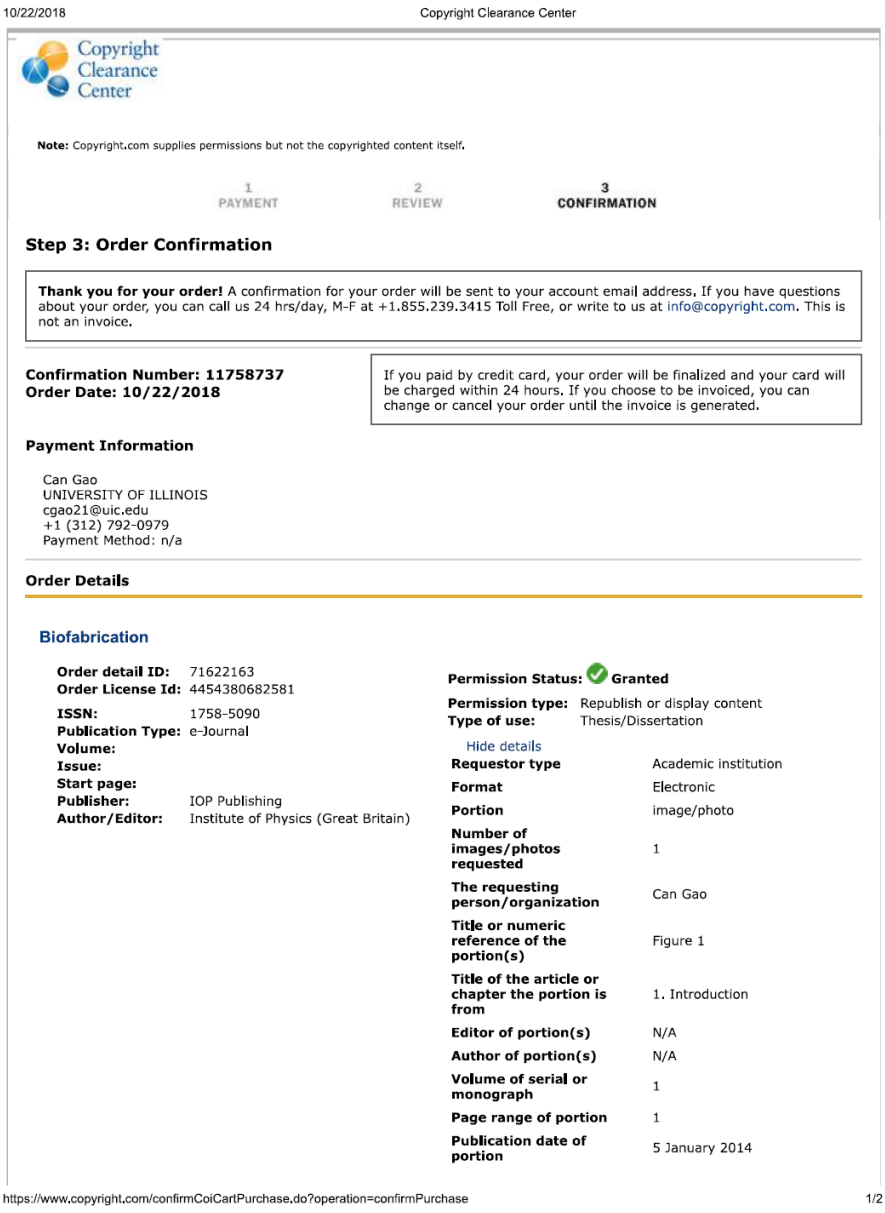

10/22/2018 Copyright Clearance Center

Copyright Clearance Center

Note: Copyright.com supplies permissions but not the copyrighted content itself.

1 PAYMENT 2 REVIEW 3 CONFIRMATION

Step 3: Order Confirmation

Thank you for your order! A confirmation for your order will be sent to your account email address. If you have questions about your order, you can call us 24 hrs/day, M-F at +1.855.239.3415 Toll Free, or write to us at info@copyright.com. This is not an invoice.

Confirmation Number: 11758737
Order Date: 10/22/2018

If you paid by credit card, your order will be finalized and your card will be charged within 24 hours. If you choose to be invoiced, you can change or cancel your order until the invoice is generated.

Payment Information

Can Gao
UNIVERSITY OF ILLINOIS
cgao21@uic.edu
+1 (312) 792-0979
Payment Method: n/a

Order Details

Biofabrication

Order detail ID:	71622163
Order License Id:	4454380682581
ISSN:	1758-5090
Publication Type:	e-Journal
Volume:	
Issue:	
Start page:	
Publisher:	IOP Publishing
Author/Editor:	Institute of Physics (Great Britain)

Permission Status: Granted
Permission type: Republish or display content
Type of use: Thesis/Dissertation

Hide details

Requestor type	Academic institution
Format	Electronic
Portion	image/photo
Number of images/photos requested	1
The requesting person/organization	Can Gao
Title or numeric reference of the portion(s)	Figure 1
Title of the article or chapter the portion is from	1. Introduction
Editor of portion(s)	N/A
Author of portion(s)	N/A
Volume of serial or monograph	1
Page range of portion	1
Publication date of portion	5 January 2014

https://www.copyright.com/confirmCoiCartPurchase.do?operation=confirmPurchase 1/2

Rights for	Main product
Duration of use	Life of current edition
Creation of copies for the disabled	no
With minor editing privileges	no
For distribution to	United States
In the following language(s)	Original language of publication
With incidental promotional use	no
Lifetime unit quantity of new product	Up to 499
Title	Study of the Effect of Air-diffusion-channel on Separation Force in Constrained Surface Stereolithography
Institution name	University of Illinois at Chicago
Expected presentation date	Dec 2018

Note: This item will be invoiced or charged separately through CCC's **RightsLink** service. More info **$ 0.00**

This is not an invoice.

Total order items: 1 **Order Total: 0.00 USD**

Permission for Figure 5

EMERALD PUBLISHING LIMITED ORDER DETAILS

Oct 22, 2018

Order Number	501438337
Order date	Oct 22, 2018
Licensed Content Publisher	Emerald Publishing Limited
Licensed Content Publication	Rapid Prototyping Journal
Licensed Content Title	Study of separation force in constrained surface projection stereolithography
Licensed Content Author	Yayue, Pan, Haiyang, He, Jie, Xu, et al
Licensed Content Date	Mar 20, 2017
Licensed Content Volume	23
Licensed Content Issue	2
Type of Use	Dissertation/Thesis
Requestor type	Academic
Author of requested content	No
Portion	Figures/table/illustration
Number of figures/tables	1
Will you be translating?	No
Format	Electronic
Geographic Rights	World rights
Order Reference Number	
Requestor Location	UNIVERSITY OF ILLINOIS 2616 S Hillock Ave Chicago, IL 60608 United States Attn: UNIVERSITY OF ILLINOIS
Publisher Tax ID	GB 665359306
Total	Not Available

Permission for Figure 11

Copyright Clearance Center RightsLink®

Home | Account Info | Help

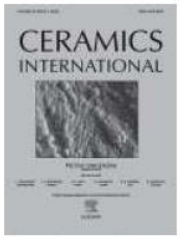

Title: Oxygen-controlled bottom-up mask-projection stereolithography for ceramic 3D printing

Author: Qin Lian,Fei Yang,Hua Xin,Dichen Li

Publication: Ceramics International

Publisher: Elsevier

Date: 1 December 2017

Logged in as:
Can Gao
UNIVERSITY OF ILLINOIS
Account #:
3001354350

LOGOUT

Order Completed

Thank you for your order.

This Agreement between UNIVERSITY OF ILLINOIS -- Can Gao ("You") and Elsevier ("Elsevier") consists of your license details and the terms and conditions provided by Elsevier and Copyright Clearance Center.

Your confirmation email will contain your order number for future reference.

printable details

License Number	4458460140728
License date	Oct 29, 2018
Licensed Content Publisher	Elsevier
Licensed Content Publication	Ceramics International
Licensed Content Title	Oxygen-controlled bottom-up mask-projection stereolithography for ceramic 3D printing
Licensed Content Author	Qin Lian,Fei Yang,Hua Xin,Dichen Li
Licensed Content Date	Dec 1, 2017
Licensed Content Volume	43
Licensed Content Issue	17
Licensed Content Pages	6
Type of Use	reuse in a thesis/dissertation
Portion	figures/tables/illustrations
Number of figures/tables/illustrations	1
Format	electronic
Are you the author of this Elsevier article?	No
Will you be translating?	No
Original figure numbers	Fig.2
Title of your thesis/dissertation	Study of the Effect of Air-diffusion-channel on Separation Force in Constrained Surface Stereolithography
Publisher of new work	University of Illinois at Chicago
Expected completion date	Dec 2018
Estimated size (number of pages)	1
Requestor Location	UNIVERSITY OF ILLINOIS 2616 S Hillock Ave

Chicago, IL 60608
United States
Attn: UNIVERSITY OF ILLINOIS

Publisher Tax ID	98-0397604
Total	0.00 USD

ORDER MORE CLOSE WINDOW

Permission for Figure 12

Copyright Clearance Center RightsLink®

Home | Account Info | Help

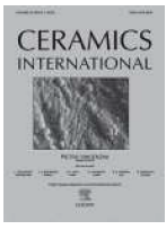

Title: Oxygen-controlled bottom-up mask-projection stereolithography for ceramic 3D printing

Author: Qin Lian,Fei Yang,Hua Xin,Dichen Li

Publication: Ceramics International

Publisher: Elsevier

Date: 1 December 2017

Logged in as:
Can Gao
UNIVERSITY OF ILLINOIS
Account #:
3001354350
LOGOUT

Order Completed

Thank you for your order.

This Agreement between UNIVERSITY OF ILLINOIS -- Can Gao ("You") and Elsevier ("Elsevier") consists of your license details and the terms and conditions provided by Elsevier and Copyright Clearance Center.

Your confirmation email will contain your order number for future reference.

printable details

License Number	4458461030602
License date	Oct 29, 2018
Licensed Content Publisher	Elsevier
Licensed Content Publication	Ceramics International
Licensed Content Title	Oxygen-controlled bottom-up mask-projection stereolithography for ceramic 3D printing
Licensed Content Author	Qin Lian,Fei Yang,Hua Xin,Dichen Li
Licensed Content Date	Dec 1, 2017
Licensed Content Volume	43
Licensed Content Issue	17
Licensed Content Pages	6
Type of Use	reuse in a thesis/dissertation
Portion	figures/tables/illustrations
Number of figures/tables/illustrations	1
Format	electronic
Are you the author of this Elsevier article?	No
Will you be translating?	No
Original figure numbers	fig.3
Title of your thesis/dissertation	Study of the Effect of Air-diffusion-channel on Separation Force in Constrained Surface Stereolithography
Publisher of new work	University of Illinois at Chicago
Expected completion date	Dec 2018
Estimated size (number of pages)	1
Requestor Location	UNIVERSITY OF ILLINOIS 2616 S Hillock Ave

Chicago, IL 60608
United States
Attn: UNIVERSITY OF ILLINOIS

Publisher Tax ID	98-0397604
Total	0.00 USD

ORDER MORE CLOSE WINDOW

Permission for Figure 30

Copyright Clearance Center RightsLink® Home Account Info Help

Title: Separation force analysis and prediction based on cohesive element model for constrained-surface Stereolithography processes

Author: Farzad Liravi,Sonjoy Das,Chi Zhou

Publication: Computer-Aided Design

Publisher: Elsevier

Date: December 2015

Published by Elsevier Ltd.

Logged in as:
Can Gao
UNIVERSITY OF ILLINOIS
Account #:
3001354350

LOGOUT

Order Completed

Thank you for your order.

This Agreement between UNIVERSITY OF ILLINOIS -- Can Gao ("You") and Elsevier ("Elsevier") consists of your license details and the terms and conditions provided by Elsevier and Copyright Clearance Center.

Your confirmation email will contain your order number for future reference.

printable details

License Number	4456651175084
License date	Oct 26, 2018
Licensed Content Publisher	Elsevier
Licensed Content Publication	Computer-Aided Design
Licensed Content Title	Separation force analysis and prediction based on cohesive element model for constrained-surface Stereolithography processes
Licensed Content Author	Farzad Liravi,Sonjoy Das,Chi Zhou
Licensed Content Date	Dec 1, 2015
Licensed Content Volume	69
Licensed Content Issue	n/a
Licensed Content Pages	9
Type of Use	reuse in a thesis/dissertation
Portion	figures/tables/illustrations
Number of figures/tables/illustrations	1
Format	electronic
Are you the author of this Elsevier article?	No
Will you be translating?	No
Original figure numbers	Figure 3
Title of your thesis/dissertation	Study of the Effect of Air–diffusion–channel on Separation Force in Constrained Surface Stereolithography
Publisher of new work	University of Illinois at Chicago
Expected completion date	Dec 2018
Estimated size (number of pages)	1
Requestor Location	UNIVERSITY OF ILLINOIS 2616 S Hillock Ave

Chicago, IL 60608
United States
Attn: UNIVERSITY OF ILLINOIS

Publisher Tax ID	98-0397604
Total	0,00 USD

ORDER MORE CLOSE WINDOW